

# Line profile variations in rapidly oscillating Ap stars: resolution of the enigma<sup>★</sup>

O. Kochukhov,<sup>1†</sup> T. Ryabchikova,<sup>2,3</sup> W. W. Weiss,<sup>3</sup> J. D. Landstreet<sup>4</sup> and D. Lyashko<sup>5</sup>

<sup>1</sup>*Department of Astronomy and Space Physics, Uppsala University, Box 515, 75120 Uppsala, Sweden*

<sup>2</sup>*Institute of Astronomy, Russian Academy of Sciences, Pyatnitskaya 48, 119017 Moscow, Russia*

<sup>3</sup>*Department of Astronomy, University of Vienna, Türkenschanzstraße 17, 1180 Vienna, Austria*

<sup>4</sup>*Department of Physics and Astronomy, University of Western Ontario, London, Ontario N6A 3K7, Canada*

<sup>5</sup>*Tavrian National University, Yaltinskaya 4, 95007 Simferopol, Crimea, Ukraine*

Accepted 2006 December 28. Received 2006 December 23; in original form 2006 November 6

## ABSTRACT

We have carried out the first survey of the pulsational line profile variability in rapidly oscillating Ap (roAp) stars. We analysed high signal-to-noise ratio time-series observations of 10 sharp-lined roAp stars obtained with the high-resolution spectrographs attached to the Very Large Telescope and Canada–France–Hawaii Telescope. We investigated in detail the variations of Pr III, Nd II, Nd III and Tb III lines and discovered a prominent change of the profile variability pattern with height in the atmospheres of all studied roAp stars. We show that, in every investigated star, profile variability of at least one rare-earth ion is characterized by unusual blue-to-red moving features, which we previously discovered in the time-resolved spectra of the roAp star  $\gamma$  Equ. This behaviour is common in rapidly rotating non-radial pulsators but is inexplicable in the framework of the standard oblique pulsator model of slowly rotating roAp stars. Using analysis of the line profile moments and spectrum synthesis calculations, we demonstrate that unusual oscillations in spectral lines of roAp stars arise from the pulsational modulation of linewidths. This variation occurs approximately in quadrature with the radial velocity changes, and its amplitude rapidly increases with height in stellar atmosphere. We propose that the linewidth modulation is a consequence of the periodic expansion and compression of turbulent layers in the upper atmospheres of roAp stars. Thus, the line profile changes observed in slowly rotating magnetic pulsators should be interpreted as a superposition of two types of variability: the usual time-dependent velocity field due to an oblique low-order pulsation mode and an additional linewidth modulation, synchronized with the changes of stellar radius. Our explanation of the line profile variations of roAp stars solves the long-standing observational puzzle and opens new possibilities for constraining geometric and physical properties of the stellar magnetoacoustic pulsations.

**Key words:** line: profiles – stars: chemically peculiar – stars: magnetic field – stars: oscillations.

## 1 INTRODUCTION

About 10–20 per cent of upper main-sequence stars are characterized by remarkably rich line spectra, often containing numerous unidentified features. Compared to the solar case, overabundances of up to a few dex are often inferred for some iron-peak and rare-earth elements (REE), whereas some other chemical elements are found to

be underabundant (Ryabchikova et al. 2004). Some of these chemically peculiar (Ap) stars also exhibit organized magnetic fields with a typical strength of a few kG. Chemical peculiarities are believed to result from the influence of the magnetic field on the diffusing ions, possibly in combination with the influence of a weak, magnetically directed wind (e.g. Babel 1992).

More than 30 cool Ap stars exhibit high-overtone, low-degree, non-radial p-mode pulsations with periods in the range of 6–21 min (Kurtz & Martinez 2000). These rapidly oscillating Ap (roAp) stars are key objects for asteroseismology, which presently is the most powerful tool for testing theories of stellar structure and evolution. The observed pulsation amplitudes of roAp stars are modulated according to the visible magnetic field structure, pointing to a defining

<sup>★</sup>Based on observations collected at the European Southern Observatory (Paranal, La Silla), at the Canada–France–Hawaii Telescope and on data retrieved from the ESO Science Archive.

†E-mail: oleg@astro.uu.se

role played by magnetic fields in exciting the oscillations and shaping the main pulsation properties. Observation of the coincidence of the magnetic field and pulsation amplitude extrema gave rise to the oblique pulsator model (OPM; Kurtz 1982). According to this phenomenological framework, the main characteristics of non-radial pulsations in roAp stars can be attributed to an oblique axisymmetric dipole ( $\ell = 1, m = 0$ ) mode, aligned with the axis of a nearly axisymmetric quasi-dipolar magnetic field.

Several theoretical investigations (e.g. Bigot & Dziembowski 2002; Saio & Gautschy 2004; Saio 2005) studied the effects of the distortion of oblique pulsation mode geometry by the global magnetic field and stellar rotation. Bigot & Dziembowski (2002) predicted that the rotational distortion of pulsation eigenmodes is represented by a superposition of spherical harmonic functions, containing substantial non-axisymmetric components, and that there is no alignment of the pulsation axis and the dipolar magnetic field. On the other hand, Saio & Gautschy (2004) and Saio (2005) disregarded effects of rotation, focusing on the detailed treatment of the interaction between p modes and a strong magnetic field. These authors find an axisymmetric pulsation structure and alignment between the magnetic field and the pulsation modes, and predict a strong confinement of pulsation amplitude to the magnetic field axis.

Recently major progress in the observational study of roAp stars was achieved by employing high time resolution spectroscopy in addition to the classical high-speed photometric measurements. Time-series spectroscopy of magnetic pulsators revealed a surprising diversity in the pulsational behaviour of different lines (e.g. Kanaan & Hatzes 1998; Kurtz, Elkin & Mathys 2006, and references therein). Detailed analyses of the bright roAp star  $\gamma$  Equ (Savanov, Malanushenko & Ryabchikova 1999; Kochukhov & Ryabchikova 2001a) demonstrated that spectroscopic pulsational variability is dominated by the lines of rare-earth ions, especially those of Pr and Nd, which are strong and numerous in the roAp spectra. On the other hand, light and iron-peak elements do not pulsate with amplitudes above  $50\text{--}100\text{ m s}^{-1}$ , which is at least an order of magnitude lower than the  $1\text{--}5\text{ km s}^{-1}$  variability observed in the lines of REE. Many other roAp stars have been found to show a very similar overall pulsational behaviour (e.g. Kochukhov & Ryabchikova 2001b; Balona 2002; Mkrtichian, Hatzes & Kanaan 2003).

The peculiar characteristics of the p-mode pulsations in roAp stars were clarified by Ryabchikova et al. (2002), who were the first to relate pulsational variability to vertical stratification of chemical elements. This study of the atmospheric properties of  $\gamma$  Equ showed that the light and iron-peak elements are enhanced in the lower atmospheric layers, whereas REE ions are concentrated in a cloud with a lower boundary at  $\log \tau_{5000} \lesssim -4$  (Mashonkina, Ryabchikova & Ryabtsev 2005). Thus, high-amplitude pulsations observed in REE lines occur in the upper atmosphere while lines of elements showing no significant variability form in the lower atmosphere. This leads to the following general picture of roAp pulsations. We observe a signature of a magnetoacoustic wave, propagating outwards with increasing amplitude through the chemically stratified atmosphere. The presence of significant phase shifts between the pulsation radial velocity (RV) curves of different REEs (Kochukhov & Ryabchikova 2001a), or even between lines of the same element (Mkrtichian et al. 2003), can be attributed to the chemical stratification effects and, possibly, to the short vertical wavelength of the running magnetoacoustic wave. These unique properties of roAp pulsations, combined with a presence of large vertical abundance gradients in the line-forming region, make it possible to resolve the vertical structure of p modes and to study propagation of pulsation waves at the level of detail previously possible only for the Sun.

The outstanding pulsational variability of REE lines in the spectra of rapidly rotating roAp stars permitted detailed mapping of the horizontal pulsation structure, leading to observational evidence that clearly favours one of the two aforementioned theoretical predictions. In fact, the short rotation periods of some roAp stars and the oblique nature of their non-radial oscillations allow pulsational monitoring from different aspect angles, thus facilitating reconstruction of the horizontal pulsation pattern. Using this unique geometrical property of roAp pulsations, and applying pulsation Doppler imaging and moment analysis techniques, Kochukhov (2004b, 2006) has successfully disentangled different harmonic contributions to the pulsation geometry of the prototype roAp star HD 83368 and for the first time obtained an independent confirmation of the alignment of non-radial pulsations and magnetic field. It was shown that the magnetoacoustic pulsations in HD 83368 are shaped as suggested by Saio & Gautschy (2004), whereas the non-axisymmetric pulsation components predicted by the theory of Bigot & Dziembowski (2002) cannot be detected.

As for the slowly rotating roAp stars, despite dramatic recent progress in understanding the vertical structure of their pulsation modes, relatively little attention has been paid to the problem of inferring the horizontal geometry of pulsations. Typically it is assumed that a horizontal cross-section of non-radial pulsation is given by an oblique axisymmetric mode of low angular degree, similar to the pulsation geometries inferred for rapidly rotating roAp stars, where periodic modulation of the geometrical aspect supplies additional information that helps to constrain the pulsation geometry. Thus, the question of systematic mode identification, central to the studies of other types of pulsating stars, has not been thoroughly investigated in the case of sharp-lined magnetic pulsators, which represent the majority of roAp stars.

Understanding rapid line profile variations (LPVs) of the slowly rotating roAp stars turns out to be a challenging task. The first observation that achieved a signal-to-noise ratio sufficient to detect profile variability (Kochukhov & Ryabchikova 2001a) demonstrated the presence of an unusual blue-to-red running feature in the residual spectra of  $\gamma$  Equ. Moreover, observations of a single-wave variability of the REE linewidth in  $\gamma$  Equ is clearly inconsistent with *any* axisymmetric pulsation geometry described by spherical harmonics (see Aerts, De Pauw & Waelkens 1992). This led Kochukhov & Ryabchikova (2001a) to attribute LPV in  $\gamma$  Equ to a non-axisymmetric  $\ell = 2\text{--}3$  non-radial mode, contrary to the classical OPM of Kurtz (1982) and in contrast to their own results for rapid rotators. Later Shibahashi et al. (2004) drew attention to the blue-to-red running wave in our time-resolved spectra of  $\gamma$  Equ. These authors showed that the observed LPV is inconsistent with spectral variability expected for any low-degree mode in a slowly rotating star and, in turn, suggested an exotic shock wave model to explain the observed rapid line profile changes.

In this study we embark on the task of detecting, characterizing and interpreting LPV in sharp-lined roAp stars. Such a study has become feasible thanks to the availability of a large amount of high-quality, time-resolved spectroscopic data for a sizable sample of roAp stars. The aim of our analysis is to derive from observations a complete picture of LPV in a number of sharp-lined roAp stars and to tackle the problem of interpretation of the REE line variability. As a result of our roAp line profile variability survey, we reveal ubiquitous asymmetric LPV in many magnetic stars. We suggest a revised OPM that recognizes the influence of stellar pulsations on turbulence in the upper atmospheric layers of roAp stars, and in this way resolves the apparent discrepancy between the axisymmetric

pulsation picture required by the standard OPM and asymmetric LPV observed in sharp-lined roAp stars.

The rest of the paper is organized as follows. Section 2 explains our choice of the target roAp stars. Section 3 describes acquisition and reduction of time-series spectra. Investigations of spectroscopic variability with residual spectra and moment analysis are presented in Section 4. Interpretation of the observations using theoretical spectrum synthesis is given in Section 5. Results of our study are summarized and discussed in Section 6.

## 2 TARGET SELECTION

The pulsational LPV pattern of a roAp star strongly depends on the orientation of the pulsation axis with respect to the line of sight, and on the magnitude of Doppler shifts due to the stellar rotation. In the slowly rotating oblique pulsators ( $V_p \gtrsim v_e \sin i$ ), the velocity field observed in REE lines is dominated by the pulsational perturbations. These roAp stars are qualitatively similar to normal non-radially pulsating stars, except that the pulsation axis obliquity  $\beta$  plays the role of the inclination angle  $i$ . When the rotational Doppler shifts exceed the local pulsational velocity over a significant fraction of the visible stellar surface ( $V_p \ll v_e \sin i$ ), the pulsational profile variability pattern changes its form, because it is now determined by a complex superposition of the rotational velocity field and oblique pulsations (Kochukhov 2004a). The behaviour of the line profile moments is also modified in comparison to the sharp-lined stars (Kochukhov 2005). These circumstances suggest that different analysis strategies are best suited for fast and slow rotators. The former should be observed over the whole rotation period and modelled taking into account the complete oblique rotator/pulsator geometry. On the other hand, one can, at least as a first approximation, neglect rotation for the latter stars and treat them as normal pulsators. The scope of the present paper is observation and interpretation of the pulsational LPV in the second, slowly rotating, group of roAp stars.

Based on our numerical simulations of the line profile and moment variations (Kochukhov 2004a, 2005), we have established  $v_e \sin i \approx 10\text{--}15 \text{ km s}^{-1}$  (the exact figure depends on the pulsation geometry and amplitude) as an upper limit of the rotational Doppler shifts which can no longer be neglected in the spectroscopic modelling of oblique non-radial pulsations. This criterion, together with the availability of high-quality spectroscopic time-series data, has defined the selection of the programme stars. Table 1 summarizes the main properties of 10 roAp stars investigated in our paper. When available, we give  $T_{\text{eff}}$ ,  $\log g$ ,  $v_e \sin i$  and the mean field modulus  $\langle B \rangle$  derived in recent model atmosphere and chemical abundance analyses (see references in Table 1). For four poorly studied roAp stars (HD 9289, HD 12932, HD 19918 and HD 134214), no detailed stud-

ies have been published, hence we adopted atmospheric parameters determined by Ryabchikova et al. (in preparation) using Strömgren photometric calibrations (Moon & Dworetzky 1985; Napiwotzki, Schoenberner & Wenske 1993). Estimates of rotational velocity and magnetic field for these four stars were obtained by fitting theoretical spectra to unblended spectral lines of different magnetic sensitivity. Details of this procedure can be found in Ryabchikova et al. (in preparation).

Time-resolved spectra are also available for several roAp stars characterized by moderate to large line broadening: HD 42659, HD 60435, HD 80316, HD 83368, HD 84041, HD 99563. These stars do not satisfy our  $v_e \sin i$  criterion or have observations of low quality (HD 60435), and were not included in the analysis.

We note that some objects selected according to their low  $v_e \sin i$  may be relatively rapid rotators seen close to one of the poles. The 3.877 d rotation period obtained by Ryabchikova et al. (2005) for HD 122970 and the 4.471-d rotational modulation found for HD 128898 (Kurtz et al. 1994; Kochukhov & Ryabchikova 2001b) hint on such a viewing geometry. Thus, an additional uncertainty may enter interpretation of the spectroscopic variability of HD 122970, HD 128898 and HD 9289 (whose rotation period is unknown, but cannot be long, given a  $v_e \sin i$  of  $10.5 \text{ km s}^{-1}$ ). Nevertheless, spectroscopic observables studied in our paper are mostly sensitive to the *projected* rotational velocity and should not be strongly distorted by the special orientation of HD 122970, HD 128898 and similar objects. Consequently, we make no explicit distinction between intrinsically slow rotators and pole-on sharp-lined stars.

The pulsation periods listed in Table 1 correspond to variability due to the dominant pulsation mode at the time of observations. In this study, we do not perform a detailed frequency analysis, and only deal with short (typically  $\approx 2\text{-h}$  long) spectroscopic time series. Therefore, possible small inaccuracies in the adopted pulsation periods have no influence on the results presented below.

## 3 OBSERVATIONS AND DATA REDUCTION

### 3.1 Echelle spectra

The main spectroscopic data set analysed in our study includes 958 observations of eight roAp stars obtained with the Ultraviolet and Visual Echelle Spectrograph (UVES) instrument at the ESO Very Large Telescope (VLT) between 2003 October 8 and 2004 March 12 in the context of the observing programme 072.D-0138 (Kurtz et al. 2006). The ESO Archive facility was used to search and retrieve science exposures and the respective calibration frames. For these observations the red arm of the UVES spectrometer was configured to observe the spectral region 4960–6990 Å

**Table 1.** Fundamental parameters of programme stars.

HD number	Other name	$T_{\text{eff}}$ (K)	$\log g$	$v_e \sin i$ ( $\text{km s}^{-1}$ )	$\langle B \rangle$ (kG)	$P$ (min)	Reference
9289	BW Cet	7840	4.15	10.5	2.0	10.52	Ryabchikova et al. (in preparation)
12932	BN Cet	7620	4.15	3.5	1.7	11.65	Ryabchikova et al. (in preparation)
19918	BT Hyi	8110	4.34	3.0	1.6	11.04	Ryabchikova et al. (in preparation)
24712	DO Eri, HR 1217	7250	4.30	5.6	3.1	6.13	Ryabchikova et al. (1997)
101065	Przybylski's star	6600	4.20	2.0	2.3	12.15	Cowley et al. (2000)
122970	PP Vir	6930	4.10	4.5	2.3	11.19	Ryabchikova et al. (2000)
128898	$\alpha$ Cir	7900	4.20	12.5	1.5	6.80	Kupka et al. (1996)
134214	HI Lib	7315	4.45	2.0	3.1	5.69	Ryabchikova et al. (in preparation)
137949	33 Lib	7550	4.30	$\leq 2.0$	5.0	8.27	Ryabchikova et al. (2004)
201601	$\gamma$ Equ	7700	4.20	$\leq 1.0$	4.1	12.21–12.45	Ryabchikova et al. (2002)

**Table 2.** Journal of time-series spectroscopic observations of roAp stars. Superscript numbers 1–6 mark different data sets of HD 201601.

HD number	Instrument/telescope	Start HJD (245 0000+)	End HJD (245 0000+)	Wavelength region (Å)	Number of exposures	Exposure time (s)	Overhead time (s)	Peak SNR
9289	UVES/VLT	2920.545 06	2920.628 81	4960–6990	111	40	25	90
12932	UVES/VLT	2921.622 34	2921.705 32	4960–6990	69	80	25	90
19918	UVES/VLT	2921.526 07	2921.609 05	4960–6990	69	80	25	100
24712	UVES/VLT	3321.657 32	3321.744 21	4960–6990	92	50	22	300
101065	UVES/VLT	3071.677 58	3071.760 32	4960–6990	111	40	25	180
122970	UVES/VLT	3069.709 77	3069.793 59	4960–6990	111	40	25	160
128898	UVES/VLT	3073.800 59	3073.882 62	4960–6990	265	1.5	25	250
134214	UVES/VLT	3070.775 71	3070.858 48	4960–6990	111	40	25	260
137949	UVES/VLT	3071.763 12	3071.845 98	4960–6990	111	40	25	350
201601	CES/ESO 3.6 m <sup>1</sup>	1381.783 44	1381.823 90	6140–6165	31	60	52	190
201601	Gecko/CFHT <sup>2</sup>	2186.706 18	2186.802 96	6543–6656	64	90	43	250
201601	Gecko/CFHT <sup>2</sup>	2186.824 56	2186.923 08	6619–6729	65	90	43	230
201601	Gecko/CFHT <sup>3</sup>	2540.722 37	2540.831 99	5283–5343	65	90	53	160
201601	Gecko/CFHT <sup>3</sup>	2540.861 01	2540.968 43	5821–5887	65	90	53	130
201601	Gecko/CFHT <sup>4</sup>	2541.854 33	2541.931 64	5821–5887	50	90	43	140
201601	Gecko/CFHT <sup>5</sup>	2542.826 88	2542.950 51	6542–6657	60	90	43	170
201601	Gecko/CFHT <sup>6</sup>	2543.823 14	2543.921 91	6104–6194	64	90	43	230

(central wavelength 6000 Å). The wavelength coverage is complete, except for a 100-Å gap centred at 6000 Å. Observations were obtained with the high-resolution UVES image slicer (slicer no 3), providing improved RV stability and giving a maximum resolving power of  $\lambda/\Delta\lambda \approx 115\,000$ .

Observations of each target cover 2 h and consist of an uninterrupted spectroscopic time series with a total number of exposures ranging from 69 to 265. The length of individual exposures was 40 or 80 s, except for the brightest roAp star HD 128898 ( $\alpha$  Cir), for which a 1.5-s exposure time was used. The ultrafast (625 kHz/4 pt) readout mode of the UVES CCDs made it possible to limit overhead to  $\approx 25$  s, thus giving a duty cycle of 70–80 per cent for the majority of targets. The signal-to-noise ratio of individual spectra is between 90 and 350, as estimated from the dispersion of the stellar fluxes in the line-free regions. Detailed description of observations for each star is given in Table 2.

The red 600-nm UVES data set was complemented by the observations of HD 24712 obtained on 2004 November 12 on DDT programme 274.D-5011. 92 time-resolved spectra were acquired with the UVES spectrometer, which was used in the 390+580-nm dichroic mode (wavelength coverage 3300–4420 and 4790–6750 Å). A detailed description of the acquisition and reduction of these data is given by Ryabchikova et al. (2007).

All échelle spectra were reduced and normalized to the continuum level with a routine specially developed by one of us (DL) for fast reduction of spectroscopic time-series observations. A special modification of the Vienna automatic pipeline for échelle spectra processing (Tsymbal, Lyashko & Weiss 2003) was developed. All bias and flat-field images were median averaged before calibration. The scattered light was subtracted using a 2D background approximation. For cleaning cosmic ray hits, we applied an algorithm which compares the direct and reversed spectral profiles. To determine the boundaries of échelle orders, the code used a special template for each order position in each row across the dispersion axis. The shift of the row spectra relative to the template was derived by a cross-correlation technique. Wavelength calibration for each roAp star was based on a single ThAr exposure, recorded immediately after the respective stellar time series. Calibration was done by a 2D approximation of the dispersion surface. An internal accuracy

of 30–40 m s<sup>-1</sup> was achieved by using several hundred ThAr lines in all échelle orders. The final step of continuum normalization and merging of échelle orders was carried out by transformation of the flat-field blaze function to the response function in each order.

The global continuum normalization was improved by iterative fitting of a smoothing spline function to the high points in the average spectrum of each star. With this procedure we have corrected an underestimate of the continuum level, unavoidable in the analysis of small spectral regions of the crowded spectra of cool Ap stars. Correct determination of the absolute continuum level is important for retrieving unbiased amplitudes of RV variability and for studying LPV. In addition to the global continuum correction, the spectroscopic time series were post-processed to ensure homogeneity in the continuum normalization of individual spectra. Each extracted spectrum was divided by the mean spectrum. The resultant ratio was heavily smoothed, and was then used to correct the continuum in the individual spectra.

### 3.2 Single-order spectra

The time-resolved observations of HD 201601 were obtained in 2001–2002 using the single-order  $f/4$  Gecko coude spectrograph with the EEV1 CCD at the 3.6-m Canada–France–Hawaii Telescope (CFHT). In total we gathered 491 observations, covering several spectral windows (see Table 2) in the 5823–6729 Å wavelength region. Observations have a resolving power, determined from the widths of a number of ThAr comparison lines, of about 115 000. In all observations of HD 201601, we used an exposure time of 90 s. Individual exposures have signal-to-noise ratio between 130 and 230.

The spectra were reduced using standard IRAF tasks. Each stellar, flat and calibration frame had a mean bias subtracted and was then cleaned of cosmic ray hits and extracted to one dimension. Extracted stellar spectra were divided by an extracted mean flat-field, and the continuum was fit with a third-order Legendre polynomial, using the same rejection parameters for all spectra so that the continuum fit is as uniform as possible. The wavelength scale was established using about 40 lines of a ThAr emission lamp, resulting in an rms scatter about the adopted pixel-wavelength polynomial (a sixth-order

Legendre polynomial) of about  $30 \text{ m s}^{-1}$ . The wavelength scale was linearly interpolated between ThAr lamp spectra taken before and after the stellar series. The spectra were not resampled to a linear wavelength spacing.

In this study we also used 31 very high resolution time-resolved observations of HD 201601 ( $\gamma$  Equ) analysed by Kochukhov & Ryabchikova (2001a). These data were obtained in 1999 with the coude echelle spectrograph (CES), fibre-linked to the Cassegrain focus of the ESO 3.6-m telescope. The highest resolution CES image slicer and the ESO CCD 38 were used, allowing us to reach a resolving power of  $\lambda/\Delta\lambda = 166\,000$  and record spectra in the 6140–6165 Å wavelength interval. We refer the reader to Kochukhov & Ryabchikova (2001a) for other details of the acquisition and reduction of the CES spectra of HD 201601.

Post-processing of the extracted spectra of HD 201601 was done consistently with the procedure adopted for UVES observations.

## 4 INVESTIGATION OF SPECTROSCOPIC VARIABILITY

### 4.1 Choice of spectral lines

Non-radial pulsations in roAp stars are best observed using lines of the rare-earth ions. Here we aim at detailed investigation of the pulsational LPV and, therefore, are limited to the analysis of variability in a few of the strongest REE lines which show the clearest signatures of oscillations. Our experience, and the results of previous studies, suggest that strong lines of Pr III and Nd III are most useful for the detection and interpretation of the rapid LPV. Therefore, we have chosen a sample of unblended doubly ionized lines of Pr and Nd. In addition, we studied a few weaker lines of Nd II and Tb III in order to sample different layers in the upper atmospheres of roAp stars and to resolve possible depth dependence of LPV. The VALD (Kupka et al. 1999) and DREAM (Biémont, Palmeri & Quinet 1999) data bases, complemented with the extended Nd III line list (Ryabchikova et al. 2006), were used as a basis for line identification. In total, we looked at 17 REE lines, including Pr III 5284, 5300, 6160, 6706 Å, Nd II 5311, 5319, 6650 Å, Nd III 5286, 5294, 5802, 5851, 6145, 6550, 6691 Å and Tb III 5505, 5847, 6323 Å. Not all lines can be studied in each star because of blending considerations, different spectral coverage of the time-resolved spectra, and the intrinsic star-to-star variation in pulsational behaviour. We preferred to analyse lines with  $\lambda \leq 6000$  Å in stars observed with UVES, whereas red REE lines with central wavelengths above 6000 Å were studied in the CFHT observations of  $\gamma$  Equ. In fact, an exhaustive investigation of all the lines listed above in each star is unnecessary because the information content of many REE features is redundant (this especially concerns the numerous strong Nd III lines).

A remarkable diversity of the pulsational amplitudes and phases observed in the spectral lines of different chemical elements indicate the importance of the depth dependence of chemical abundances and of pulsation wave properties in roAp atmospheres. Taking this into account, we expect to find a significant depth dependence of the pulsational LPV. This is why it is important to study variability in diverse REE lines, and to associate observed LPV patterns with specific atmospheric layers. However, the question of the formation depth of REE lines in the atmospheres of roAp stars is an extremely complex one. Ideally it should be addressed with detailed non-local thermodynamic equilibrium (NLTE) chemical stratification calculations (Mashonkina et al. 2005), possibly taking into account the anomalous structure of the upper atmospheres of cool Ap stars (Kochukhov, Bagnulo & Barklem 2002). Such an analysis is

extremely demanding in terms of computing time and input physics, and up to now has been carried out only for Nd II and Nd III in two representative roAp stars (Mashonkina et al. 2005). The results of these elaborate NLTE-chemical stratification calculations show that line intensity can be used as a good proxy for the *relative* formation depth of spectral features belonging to the same element. For instance, weaker singly ionized Nd lines are formed deeper than strong Nd III lines. On the other hand, the intensity of the lines of different elements is not a reliable indicator of the formation depth because there is no reason to assume that vertical stratification is the same for all REE species. Nevertheless, one can still assign an approximate relative formation depth to the lines of different REEs based on phases of RV variability. In the framework of a running magnetoacoustic wave which propagates outwards, the lines showing later RV maximum are formed higher in the atmosphere. We will use this property for intercomparison of the results obtained for Pr, Nd and Tb lines. One has to keep in mind, however, that different horizontal sampling of the pulsation velocity field due to dissimilar spotted distribution of different REEs may distort this phase-depth relation. Moreover, any judgment about formation heights based solely on the time of the velocity extrema becomes meaningless when the vertical p-mode structure is dominated by the standing wave component, and pulsation nodes with the associated  $180^\circ$  phase change are observed in the line-forming region. One roAp star included in our sample, HD 137949, is known to show this behaviour (Mkrtychian et al. 2003).

### 4.2 Residual spectra

We start analysis of the pulsational LPV in roAp stars by investigating the behaviour of the residual spectra as a function of pulsation phase. This is the most general approach to characterize LPV of pulsating stars and, because the whole information content of the line profile changes is considered, this method may be preferable in some cases to analysis of average secondary quantities, such as line profile moments and bisectors. On the other hand, analysis of the residual spectra has a drawback, in that it is impossible to directly relate features in the LPV pattern to physical properties of non-radial pulsations. LPV represents a result of a non-trivial convolution of the intrinsic stellar line profiles and velocities due to pulsation and stellar rotation. Therefore, credible interpretation of the residual profile variation is possible only with the help of spectrum synthesis calculations which adequately describe the aforementioned effects.<sup>1</sup>

Investigation of the residual spectra is feasible only for time-resolved observations of sufficient quality. The signal-to-noise ratio of the time-series spectra of roAp stars available to us is quite uneven, which precludes direct detection of the periodic LPV in fainter stars (about half of our sample). To circumvent this difficulty, we developed a special spectral co-addition procedure. First, we derive an average spectrum for each star and subtract it from the individual observations. Then pulsation phases are computed using the periods listed in Table 1. Observations with similar phases are averaged. We typically divided the pulsation cycle into 10 phase bins, except for the CFHT and ESO 3.6-m  $\gamma$  Equ data sets where 11 and 13 phase bins were used, respectively.

<sup>1</sup> In this context we note that the assertion by Shibahashi et al. (2004) that certain features of the LPV observed in  $\gamma$  Equ by Kochukhov & Ryabchikova (2001a) can be interpreted in terms of the pulsation velocity amplitude is erroneous.

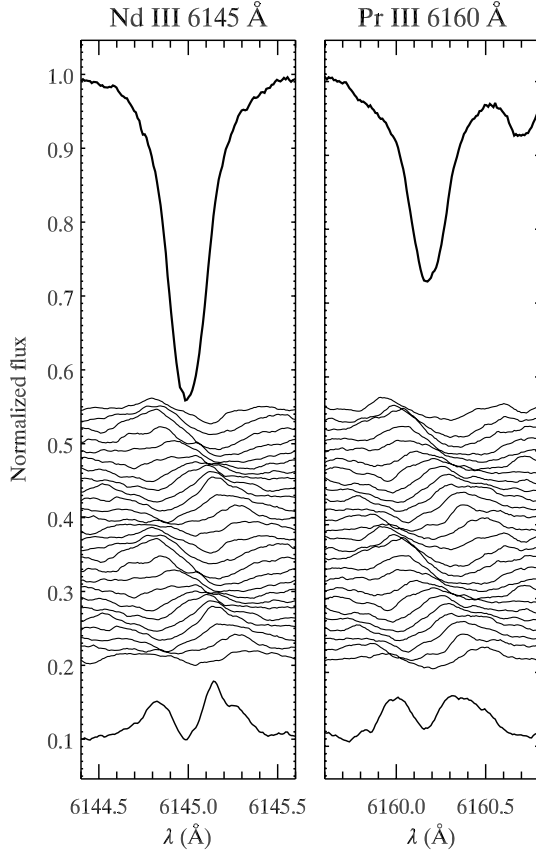


**Figure 1.** Profile variations of the Nd III 6145 Å and Pr III 6160 Å lines in the CES observations of  $\gamma$  Equ obtained on 1999 June 22. The average spectrum is plotted in the upper part of each panel. The difference spectra as a function of pulsation phase are presented in the middle part. Observations for consecutive pulsation phases are shifted in the vertical direction, and each phase is shown twice. The bottom curve presents the wavelength dependence of the standard deviation (expanded by a factor of 10).

Variation of the residual profiles of the Nd III 6145 Å and Pr III 6160 Å lines in  $\gamma$  Equ, processed with our phase binning procedure, is illustrated in Fig. 1. In this and other similar plots we show the average line profile on top, the time series of the difference spectra is plotted in the middle (with time increasing downwards), and the standard deviation profile is shown at the bottom of the plot. Comparison of the binned LPV presented in Fig. 1 with the profile variations in the original observations (see Fig. 1 in Kochukhov & Ryabchikova 2001a) shows very good agreement. This indicates that application of the phase binning procedure to the time-resolved spectra of roAp stars is able to enhance S/N while retaining the original LPV pattern. As was observed by Kochukhov & Ryabchikova (2001a), we find that LPV of the Nd III and Pr III lines studied is asymmetric, and is dominated by the blue-to-red moving feature.

The LPV pattern detected in the CFHT observations of  $\gamma$  Equ is shown in Fig. 2. This  $\gamma$  Equ data set is unique in that it shows an exceptionally high amplitude of the pulsational variability (RV semi-amplitude of up to  $1 \text{ km s}^{-1}$  for a number of REE lines) compared to all other observations of  $\gamma$  Equ reported in the literature (Kochukhov & Ryabchikova 2001a; Kochukhov, Ryabchikova & Piskunov 2004; Savanov et al. 2005). Fig. 2 compares behaviour of the core of H $\alpha$ , Pr III 6706 Å, Nd III 6550, 6691 Å and Nd II 6650 Å. (Two plots are shown for the latter line, corresponding to observations in the two

consecutive time series recorded during the same night.) One can see a clear difference in the LPV pattern displayed by the H $\alpha$  core, Nd II 6650 Å and Nd III 6691 Å on the one hand and by the Nd III 6550 Å, Pr III 6706 Å features on the other hand. The first group of lines shows nearly symmetric, S-shaped variability, whereas the two lines from the second group behave similarly to the Nd III 6145 Å and Pr III 6160 Å lines in Fig. 1, and show a blue-to-red moving wave. We suggest that this difference reflects the depth variation of the pulsational LPV pattern. Sophisticated line formation calculations (Mashonkina et al. 2005) predict that the absorption in the Nd II 6650 Å line originates at the bottom of the Nd-rich layer. The Nd III 6691 Å line is one of the few doubly ionized Nd lines whose formation depth overlaps with that of Nd II. This is confirmed by a rather small delay ( $\Delta\varphi = 0.08$ , hereafter we give phases and phase differences in units of pulsation period) of its RV maximum relative to the RV variation of Nd II 6650 Å. In contrast, the strong line Nd III 6550 Å forms substantially higher and shows a large phase delay ( $\Delta\varphi = 0.21$ ). Detailed NLTE radiative transfer calculations are not yet available for Pr III, but, given that the weak Pr III 6706 Å line has a phase lag similar to that of Nd III, its effective formation height should not differ much. Indeed, we see qualitatively the same LPV pattern for this Pr III feature and for Nd III 6550 Å.

The formation depth of the H $\alpha$  core is difficult to estimate. Based on its symmetric LPV pattern, we expect the H $\alpha$  core to form below the Nd-rich layer, in agreement with the proposed depth dependence of LPV in metal lines. Nevertheless, the large intrinsic Doppler width of the H $\alpha$  core does not permit a straightforward comparison with the variability detected in REE lines. In addition, the pulsational changes of the H $\alpha$  core are too low in some of the roAp stars included in our study. For these reasons, we refrain from detailed analysis of the H $\alpha$  profile behaviour in this paper.

The CFHT observations of  $\gamma$  Equ discussed in this section constitute the first detection of the depth variation of the pulsational LPV pattern in a roAp star. Moreover, to our knowledge, such behaviour has not previously been observed in any main-sequence non-radially pulsating star. We conclude that the pulsational LPV changes significantly within the REE-enriched cloud in the upper atmosphere of  $\gamma$  Equ: the symmetric, S-shaped LPV pattern of the lines from deeper layers is replaced by asymmetric, blue-to-red moving features in the LPV of lines formed higher up.

For the analysis of the REE line profile variability in our main UVES data set of nine roAp stars we used the Nd II 5319 Å, Nd III 5294 Å, Pr III 5300 Å and Tb III 5847 Å lines. The Nd II feature is sufficiently strong to be observed in all stars and is formed at the bottom of the Nd-rich cloud. The 5294 Å line is one of the strongest Nd III lines in the optical spectra of cool Ap stars. This line samples high atmospheric layers. In general, nothing can be said about the formation heights of the chosen lines of doubly ionized Pr and Tb because they depend on currently unknown details of stratification of these REE species in individual stars.

Fig. 3 shows residual profile variation for the Nd II 5319 Å line. Among the nine roAp stars presented in this plot, seven show a symmetric or nearly symmetric (HD 19918), S-shaped LPV pattern similar to the one which we found for Nd II lines in  $\gamma$  Equ. HD 9289 shows a weak red-to-blue moving wave – an odd behaviour which is not seen in any other star. Time series of the residual spectra are inconclusive for HD 137949 because at the heights sampled by Nd II 5319 Å, a pulsation node is observed in this star and the variation is dominated by the first harmonic of the main frequency. However, the H $\alpha$  core in HD 137949 has symmetric variability (Kurtz et al. 2004), quite similar to the behaviour of Nd II in the majority of the roAp stars studied.

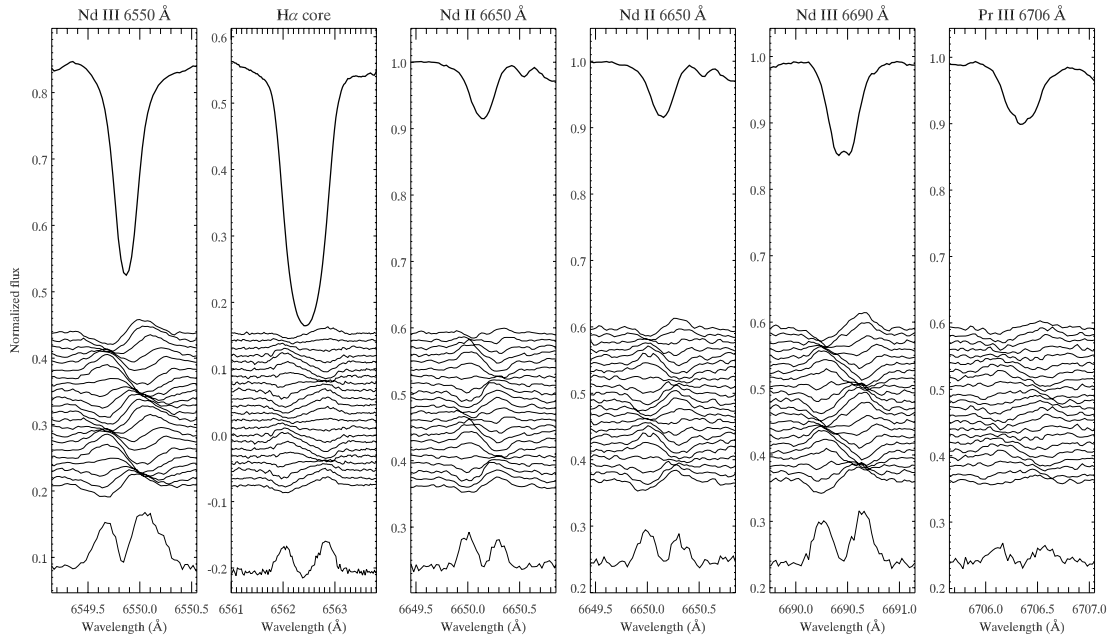


**Figure 2.** Profile variations of the Nd III 6550 Å, H $\alpha$  core, Nd II 6650 Å, Nd III 6690 Å and Pr III 6706 Å lines in the CFHT observations of  $\gamma$  Equ obtained on 2001 October 4. The layout of the figure is similar to that of Fig. 1.

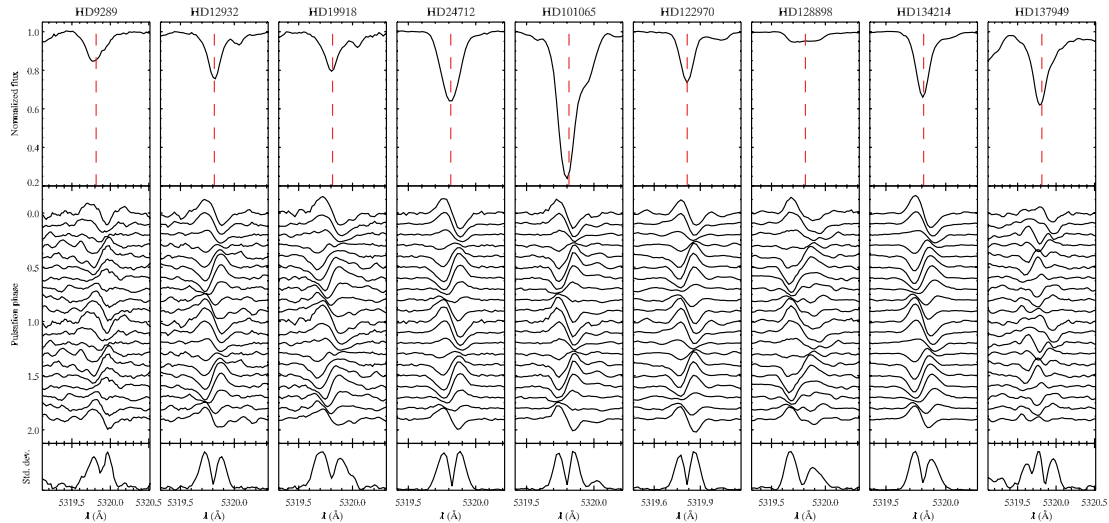


**Figure 3.** Profile variations of the Nd II 5319 Å line for nine roAp stars. The layout of the figure is similar to that of Fig. 1, except that here an arbitrary intensity scale is used for the residual and standard deviation spectra. The vertical dashed lines indicate position of line centres.

Considering variation of the Nd III 5294 Å line (Fig. 4), we detect a well-developed LPV pattern with blue-to-red moving waves in HD 9289, HD 12932, HD 19918, HD 24712, HD 128898, HD 134214 and HD 137949. The phase lag of this Nd III line with respect to the RV changes of Nd II 5319 Å is typically in the range 0.17–0.22, but smaller (0.15–0.17) for HD 24712 and HD 134214. These two stars exhibit LPV of a transitional type: it is possible to trace a blue-to-red moving wave; however, the latter is not continuous, but formed by two separate ‘bumps’ in the time-sequence of the residual spectra. The two cooler stars, HD 101065 and HD 122970, retain the S-shaped LPV which was present in the Nd II 5319 Å line. Remarkably, these two stars also show a much smaller phase lag ( $\Delta\varphi = 0.01$ – $0.04$ ) between Nd III and Nd II compared to the rest of the roAp star sample. Either the formation heights of the Nd II and

Nd III lines are less different in cooler roAp stars due to a special form of Nd stratification, or the pulsation wave structure sampled by the Nd lines is dominated by a standing wave. It is worth mentioning that abundance analysis of HD 101065 (Cowley et al. 2000) provides no evidence of the Nd II–Nd III abundance anomaly found in other roAp stars.

The variation of the Pr III 5300 Å line is illustrated in Fig. 5. The negligible phase lag of this REE line with respect to Nd III 5294 Å in HD 9289, HD 12932 and HD 19918 corresponds to essentially the same LPV behaviour as shown by the Nd III line. Thus, we may suggest that Pr III and Nd III lines in these stars form in similar layers – a situation reminiscent of the Pr III/Nd III line variation in  $\gamma$  Equ. HD 24712, HD 128898 and HD 134214 show a larger phase lag ( $\Delta\varphi = 0.06$ – $0.11$ ) and a stronger asymmetry in the Pr III line

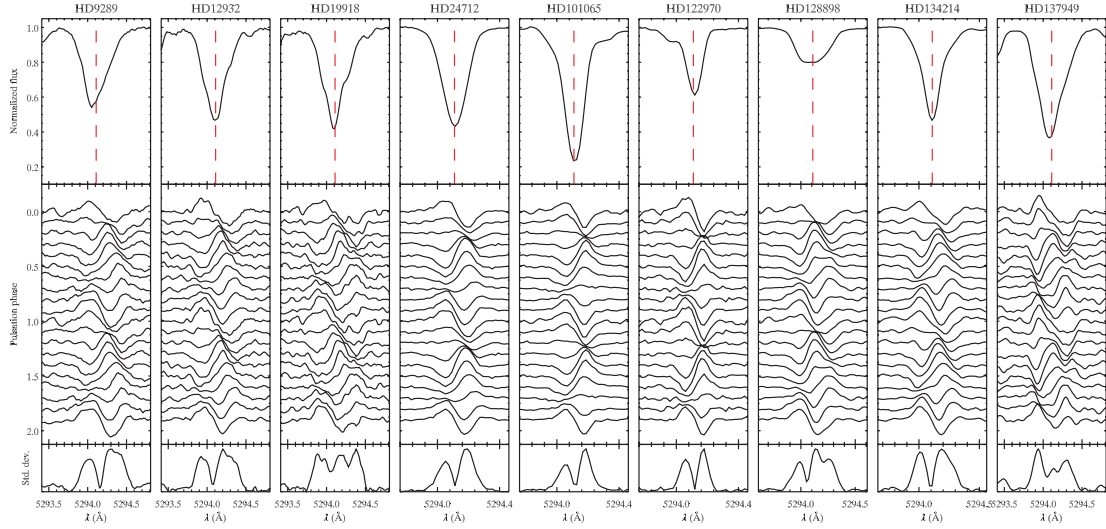


**Figure 4.** Profile variations of the Nd III 5294 Å line for nine roAp stars. The layout of the figure is similar to that of Fig. 3.

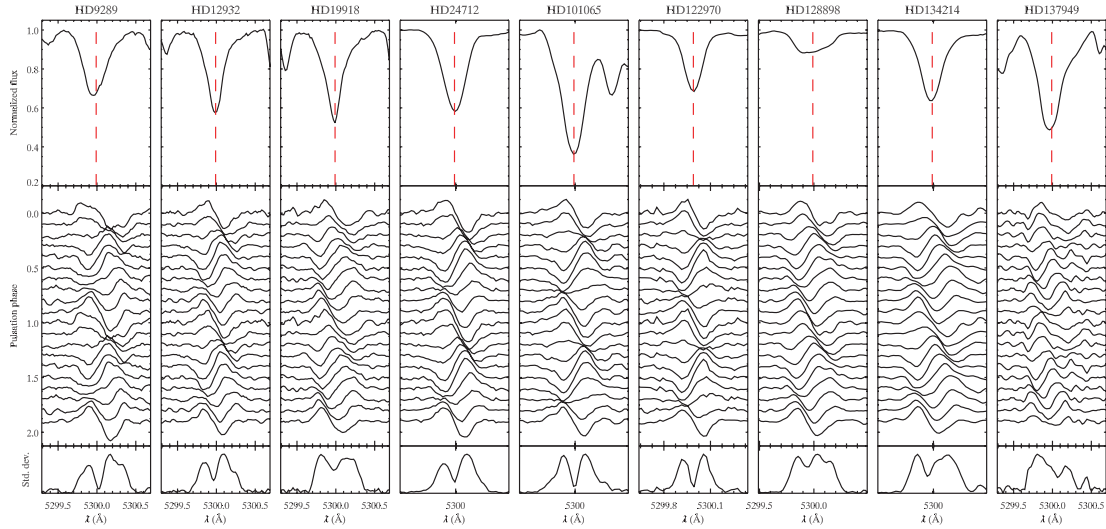


**Figure 5.** Profile variations of the Pr III 5300 Å line for nine roAp stars. The layout of the figure is similar to that of Fig. 3.

variability. HD 101065 and HD 122970 continue to show symmetric LPV pattern. Analysis of the Pr III 5300 Å line in HD 137949 is complicated by the low RV amplitude and by the presence of harmonic oscillations. Nevertheless, blue-to-red moving features are still visible in the time evolution of the residual spectra constructed for this star.

Finally, we investigated variation of the Tb III 5847 Å line. Its pulsational behaviour is diverse in the studied sample of roAp stars. Large pulsational amplitude and significant phase shifts of this line in some stars may indicate that Tb III probes atmospheric layers above those to which Nd III and Pr III lines are sensitive. Fig. 6 shows variation of Tb III 5847 Å in four cooler roAp stars (HD 24712, HD 101065, HD 122970, HD 134214). A very clear asymmetric LPV and significant (0.16–0.23) phase delay with respect to Pr III 5300 Å is found for HD 24712, HD 101065 and HD 134214. Variation of the Tb III line in HD 122970 exhibits a transitional behaviour (cf. the Nd III 5294 Å variation in HD 134214), showing the first signature of the blue-to-red running waves.

Our survey of the pulsational LPV in Nd, Pr and Tb lines in nine roAp stars reveals ubiquitous signatures of the depth variation of the profile variability pattern in every star. This corroborates results obtained for  $\gamma$  Equ and shows that a large vertical gradient of the amplitude and phase of pulsation waves observed in the atmospheres of roAp stars is associated with a similar rapid change of the LPV pattern. All stars, except HD 9289, show symmetric LPV in deeper layers. All stars, without exception, ultimately develop asymmetric LPV in the upper atmospheric region. This behaviour is apparently correlated with  $T_{\text{eff}}$ : we find that hotter stars (HD 9289, HD 12932, HD 19918, HD 128898, HD 137949) develop interesting asymmetric LPV pattern lower (in the layers sampled by Nd III 5294 Å) than cooler stars (HD 24712, HD 101065, HD 122970, HD 134214). We also identified a characteristic change in the shape of the standard deviation profile associated with the transition from symmetric to asymmetric LPV. In the former case the blue and red peaks in the standard deviation spectra are well separated and there is almost no variation in the line core. In the latter case, the two peaks are often

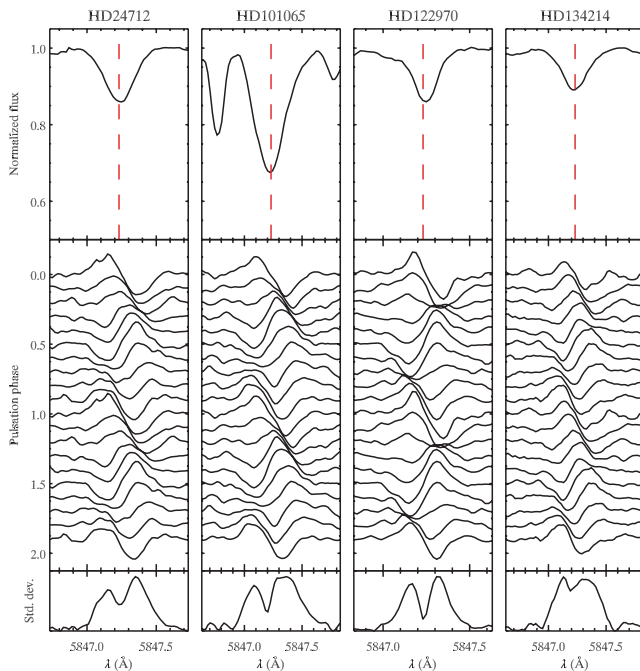


**Figure 6.** Profile variations of the Tb III 5847 Å line for four cool roAp stars. The layout of the figure is similar to that of Fig. 3.

merged together and some residual intensity changes are observed in the line centre (e.g. Pr III 5300 Å in HD 19918 and HD 134214, Tb III 5847 Å in HD 24712 and HD 134214).

### 4.3 Line profile moments

Interpretation of the line profile moment variation of slowly rotating pulsating stars is a useful pulsation mode diagnostic technique (Balona 1986; Aerts et al. 1992; Briquet & Aerts 2003). Many studies have successfully utilized analysis of the pulsational behaviour of the low-order line profile moments to determine oscillation frequencies and to identify pulsation modes. Recently, Kochukhov (2005) has generalized the moment method to treat pulsations arbitrarily inclined with respect to the stellar rotation axis. This modification of the moment technique is essential for its application to roAp stars.

In the present study, we complement direct analysis of the pulsational LPV based on residual spectra with the study of pulsational perturbation of the REE line profile moments. These quantities are defined according to the following relation (Aerts et al. 1992):

$$\langle V^j \rangle = \sum_i \left[ \frac{c(\lambda_i - \langle \lambda \rangle)}{\langle \lambda \rangle} \right]^j (1 - S_i) / \sum_i (1 - S_i), \quad (1)$$

where  $\langle V^j \rangle$  is the line profile moment of  $j$ th order,  $\lambda_i$  and  $S_i$  are the wavelength and normalized intensity at the  $i$ th pixel of observed spectrum and  $c$  is the speed of light. Moments are computed with respect to the wavelength ( $\lambda$ ) corresponding to the centre of gravity of absorption feature in the average spectrum. The first moment  $\langle V \rangle$  represents a measure of RV, whereas the second moment  $\langle V^2 \rangle$  is related to linewidth. The sum in equation (1) is cut off when intensity reaches continuum level or at the point when blending by the neighbouring lines becomes significant. To improve the accuracy of the calculation of moments with equation (1), we have resampled the spectra of roAp stars into a fine wavelength grid with the help of cubic splines. In each star the pulsational variation of the first

and second moments was investigated for a set of unblended lines of Pr III, Nd II, Nd III and Tb III.

Time series of the line profile moments are analysed with the least-squares fitting method in order to characterize variation at the principal frequency and its first harmonic, and to extract the respective pulsation phases. Moment variation is approximated by the expression

$$\langle V^j \rangle = V_0(t - t_0) + \sum_{i=1}^2 V_{ji} \cos \{2\pi[i(t - t_0)/P - \varphi_{ji}]\}. \quad (2)$$

Here the first term takes into account possible drift of the spectrograph's zero-point. The HJD of the first exposure of the star at a given night (see Table 2) was chosen as the reference time  $t_0$ .  $V_{ji}$  and  $\varphi_{ji}$  are, respectively, the amplitude and phase of the  $j$ th moment variation with the main period ( $i = 1$ ) and half the main period ( $i = 2$ ). With the minus sign in front of  $\varphi_{ji}$  a larger phase corresponds to a later time of maximum of  $\langle V \rangle$  or  $\langle V^2 \rangle$ . This phase convention is natural when discussing effects of the outward propagation of pulsation waves in the atmospheres of roAp stars. The pulsations periods in equation (2) are fixed to the values listed in Table 1.

From theoretical considerations (Aerts et al. 1992; Kochukhov 2005) it is expected that the RV of the star exhibiting low-amplitude linear non-radial pulsations changes sinusoidally, whereas variation of the second moment may contain a significant contribution of the first harmonic. The amplitude ratio  $V_{21}/V_{22}$  characterizing the overall shape of the  $\langle V^2 \rangle$  phase curve is very sensitive to the horizontal structure of the pulsation velocity field. However, possible non-linearities may lead to a non-zero harmonic contribution to the first moment variation and could distort the second moment amplitude ratio diagnostics. Thus, in order to assess possible contribution of the intrinsic harmonic variability, we fitted the same expression given by equation (2) to the time series of both  $\langle V \rangle$  and  $\langle V^2 \rangle$ .

An example of the moment analysis for several REE lines in HD 19918 and HD 101065 is displayed in Fig. 7. The first and second moment measurements are compared with the best-fitting cosine curves computed according to equation (2). Numerical results of fitting the first and second moment variability are compiled in Tables 3 and 4 for the roAp stars observed with UVES and in Table 5 for HD 201601. We have verified that the pulsational behaviour of the latter star does not change significantly in the course of individual observing nights. Thus, we consider moment measurements obtained in different wavelength regions observed on the same nights to be part of the same data set. This gives us six groups of time-resolved spectra, referred to by the numbers 1–6 in Tables 2 and 5.

In the remaining part of this section we explore various trends in the amplitudes and phases of moment variation and relate these quantities to the LPV of REE lines discussed in Section 4.2. We start by noting that majority of the roAp stars in our sample show nearly sinusoidal RV variation. Marginally significant non-zero  $V_{12}$  amplitudes are obtained only for a few REE lines in HD 9289, HD 101065, HD 122970 and HD 128898. Nevertheless, for all these objects condition  $V_{11} \gg V_{12}$  is fulfilled, indicating that possible non-linearity or a contribution arising from the resonantly excited harmonic oscillation is negligible. Thus, the presence of harmonic variation of the second moment and the amplitude ratio  $V_{21}/V_{22}$  retains their value as mode structure diagnostics. An atypical behaviour is found for HD 137949. A sizable fraction of REE lines in this star shows significant, in some cases dominant, double-wave RV variation and correspondingly have large  $V_{12}$  amplitude. In this situation, the origin of harmonic variability of  $\langle V^2 \rangle$  is ambiguous.

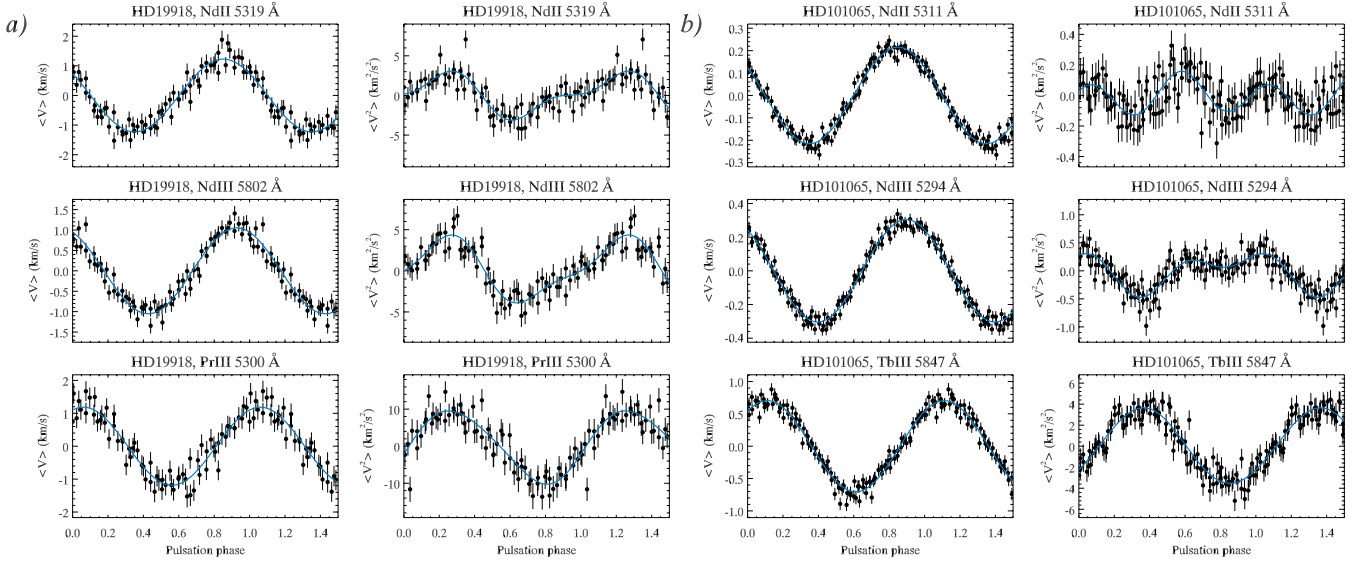


**Figure 7.** Variation of line profile moments for rare-earth lines in (a) HD 19918 and (b) HD 101065. For each star the behaviour of the first ( $\langle V \rangle$ ) (left-hand panels) and second ( $\langle V^2 \rangle$ ) (right-hand panels) profile moments is presented. Symbols show the moment measurements as a function of pulsation phase. The curves illustrate a fit including variation with the principal frequency and its first harmonic.

Following arguments presented in Section 4.1, we use the phase  $\varphi_{11}$  of RV fluctuations as a proxy of the relative formation height for REE lines. For pulsation waves propagating outwards in the radial direction, a larger RV phase corresponds to a later time of maximum velocity, which suggests a higher physical location of the line-forming region of the REE ion.

For all stars except HD 137949 we discover a dramatic change of the second moment amplitude  $V_{21}$  with height. This trend is evident from inspection of Fig. 7 for HD 19918 and HD 101065. The Nd II lines from deeper layers often exhibit large, or at least measurable harmonic variation of  $\langle V^2 \rangle$ . As the pulsation wave propagates towards higher layers, the  $V_{21}$  amplitude increases steeply and the shape of  $\langle V^2 \rangle$  phase curve transforms from a low-amplitude, predominantly double wave to a large-amplitude, mostly single wave. This tendency is summarized for all stars in Figs 8 and 9. We find a persistent increase of the principal frequency component in the  $\langle V^2 \rangle$  variation with increasing phase  $\varphi_{11}$ . Typically, Nd II lines have low  $V_{21}$  amplitude; this parameter increases in strong Nd III lines, continues increasing for Pr III and finally reaches maximum in Tb III (HD 12932, HD 24712, HD 101065, HD 122970, HD 128898, HD 134214). For a few stars (HD 9289, HD 19918 and HD 201601) where Tb III lines do not show large-amplitude variability of  $\langle V^2 \rangle$  the  $V_{21}$  amplitude maximum occurs in Pr III lines.

Comparing the inferred depth dependence of the second moment variation with the line-to-line changes of LPV pattern, we discovered a remarkable correspondence between high-amplitude, single-wave pulsational variability of  $\langle V^2 \rangle$  and the presence of a blue-to-red wave pattern in the LPV. Detailed intercomparison of the residual profile time series displayed in Figs 3–6 and the moment fitting results reveals that all those lines, in particular Pr III and Tb III, showing asymmetric LPV are invariably characterized by a large  $V_{21}$  amplitude and high  $V_{21}/V_{11}^2$  ratio. The latter parameter reaches a value of 10–15 for Pr III and Tb III in most stars. The depth variation of LPV pattern and  $V_{21}$  amplitude is also consistent. The two stars, HD 101065 and HD 122970, that develop asymmetric LPV late and show it prominently only in the Tb III lines also exhibit less persistent single-wave second moment changes and have lower  $V_{21}/V_{11}^2$  ratios

(2–7). Thus, an important conclusion emerging from our analysis of the first and second moment variation with pulsation phase is that a large-amplitude, single-wave behaviour of  $\langle V^2 \rangle$  and asymmetric LPV pattern are closely related and probably have the same physical origin. We stress that this correlation between the two distinct characteristics of the roAp spectroscopic variability is universal and is found in all stars where intrinsic harmonic variability is low enough not to distort the moment technique diagnosis. Consequently, any theory purporting to explain the asymmetric LPV pattern of sharp-lined roAp stars must also reproduce the main features of the moment behaviour.

Further insight into pulsational linewidth perturbations is obtained by considering the phase shift between the dominant single-wave variability of  $\langle V \rangle$  and  $\langle V^2 \rangle$ . In Figs 8 and 9 we plot the phase delay,  $\varphi_{21} - \varphi_{11}$ , of the second moment with respect to the phase  $\varphi_{11}$  of the RV curve. The value of this phase lag is diverse for different groups of spectral lines, and no consistent depth dependence is found. However, an interesting coherency is found for the numerical value of  $\varphi_{21} - \varphi_{11}$  in lines with dominant single-wave variation of the second moment. Using lines of Pr III and Tb III (for HD 201601 the Nd III lines are also considered) which are sensitive to pulsations in the outermost stellar layers, we find that  $\varphi_{21} - \varphi_{11}$  is always positive (see average values of the phase lag listed in Tables 2–5). This means that the  $\langle V^2 \rangle$  maximum occurs later in time compared to the RV maximum. Furthermore, the  $\varphi_{21} - \varphi_{11}$  parameter spans a small range of values between 0.19 and 0.28. (The few exceptions include HD 9289, which has  $\langle \varphi_{21} - \varphi_{11} \rangle = 0.09$ , and one  $\gamma$  Equ data set with  $\langle \varphi_{21} - \varphi_{11} \rangle = 0.15$ ). For seven out of 10 stars studied,  $\langle \varphi_{21} - \varphi_{11} \rangle$  is consistent within  $1\sigma$  confidence level with exactly one-quarter period phase lag between RV and  $\langle V^2 \rangle$ . For two stars (HD 24712 and HD 134214) the phase lag is consistent with the value of 0.25 at a  $2\text{--}3\sigma$  level.

How does one interpret a systematic quarter-period delay between the variation of RV and linewidth? We recall that, in the absence of significant non-linearities and non-adiabatic effects in stellar pulsations, the velocity is shifted by 0.25 of the period with respect to radius changes. The negative extremum of  $\langle V \rangle$  corresponds to

**Table 3.** Results of the least-squares fitting of the first and second moment variation of the REE lines in HD 9289, HD 12932, HD 19918, HD 24712 and HD 101065. The columns give line identification, amplitude and phase ( $V_{11}$ ,  $\varphi_{11}$ ) for the  $\langle V \rangle$  variation at the main frequency and amplitude of the  $\langle V \rangle$  variability ( $V_{12}$ ) at the first harmonic. The same quantities are listed for the second moment ( $\langle V^2 \rangle$ ). Amplitudes are measured in  $\text{km s}^{-1}$  for  $\langle V \rangle$  and in  $\text{km}^2 \text{s}^{-2}$  for  $\langle V^2 \rangle$ , phases are given in units of the pulsation period. The HD number of the star is followed by the phase difference  $\varphi_{21} - \varphi_{11}$ , estimated using the lines of Pr III and Tb III.

Ion	$\lambda$ ( $\text{\AA}$ )	$V_{11}$ ( $\text{km s}^{-1}$ )	$\langle V \rangle$ $\varphi_{11}$	$V_{12}$ ( $\text{km s}^{-1}$ )	$V_{21}$ ( $\text{km}^2 \text{s}^{-2}$ )	$\langle V^2 \rangle$ $\varphi_{21}$	$V_{22}$ ( $\text{km}^2 \text{s}^{-2}$ )
HD 9289, ( $\varphi_{21} - \varphi_{11}$ ) = $0.09 \pm 0.04$							
Pr III	5284	$0.549 \pm 0.024$	$0.673 \pm 0.007$	$0.048 \pm 0.024$	$3.738 \pm 0.315$	$0.742 \pm 0.013$	$0.720 \pm 0.316$
Nd III	5286	$0.518 \pm 0.036$	$0.524 \pm 0.011$	$0.024 \pm 0.036$	$3.087 \pm 0.348$	$0.501 \pm 0.018$	$0.143 \pm 0.350$
Nd III	5294	$0.603 \pm 0.031$	$0.712 \pm 0.008$	$0.068 \pm 0.031$	$4.934 \pm 0.498$	$0.786 \pm 0.016$	$0.675 \pm 0.497$
Pr III	5300	$0.750 \pm 0.033$	$0.689 \pm 0.007$	$0.117 \pm 0.033$	$5.980 \pm 0.492$	$0.755 \pm 0.013$	$0.696 \pm 0.492$
Nd II	5311	$0.487 \pm 0.086$	$0.584 \pm 0.028$	$0.016 \pm 0.087$	$3.921 \pm 0.863$	$0.352 \pm 0.035$	$1.482 \pm 0.862$
Nd II	5319	$0.629 \pm 0.057$	$0.538 \pm 0.014$	$0.121 \pm 0.057$	$2.890 \pm 0.581$	$0.486 \pm 0.032$	$1.013 \pm 0.583$
Tb III	5505	$0.533 \pm 0.029$	$0.676 \pm 0.009$	$0.057 \pm 0.029$	$3.274 \pm 0.306$	$0.744 \pm 0.015$	$0.562 \pm 0.306$
Nd III	5802	$0.596 \pm 0.035$	$0.565 \pm 0.009$	$0.029 \pm 0.035$	$3.811 \pm 0.474$	$0.571 \pm 0.020$	$1.101 \pm 0.475$
Tb III	5847	$0.451 \pm 0.082$	$0.641 \pm 0.029$	$0.109 \pm 0.082$	$2.531 \pm 0.755$	$0.781 \pm 0.048$	$1.209 \pm 0.752$
Nd III	5851	$0.653 \pm 0.043$	$0.559 \pm 0.011$	$0.025 \pm 0.043$	$4.133 \pm 0.652$	$0.564 \pm 0.025$	$1.364 \pm 0.651$
HD 12932, ( $\varphi_{21} - \varphi_{11}$ ) = $0.23 \pm 0.02$							
Pr III	5284	$1.052 \pm 0.039$	$0.210 \pm 0.006$	$0.015 \pm 0.039$	$7.129 \pm 0.562$	$0.413 \pm 0.012$	$1.022 \pm 0.558$
Nd III	5286	$0.960 \pm 0.040$	$0.033 \pm 0.007$	$0.022 \pm 0.040$	$1.592 \pm 0.208$	$0.285 \pm 0.021$	$0.491 \pm 0.206$
Nd III	5294	$0.843 \pm 0.030$	$0.223 \pm 0.006$	$0.050 \pm 0.030$	$6.290 \pm 0.339$	$0.466 \pm 0.009$	$0.276 \pm 0.335$
Pr III	5300	$1.199 \pm 0.037$	$0.184 \pm 0.005$	$0.082 \pm 0.037$	$8.512 \pm 0.428$	$0.435 \pm 0.008$	$0.772 \pm 0.426$
Nd II	5311	$0.734 \pm 0.042$	$0.975 \pm 0.009$	$0.088 \pm 0.042$	$0.830 \pm 0.181$	$0.394 \pm 0.035$	$0.258 \pm 0.181$
Nd II	5319	$1.012 \pm 0.032$	$0.005 \pm 0.005$	$0.023 \pm 0.031$	$1.388 \pm 0.162$	$0.415 \pm 0.018$	$0.280 \pm 0.161$
Tb III	5505	$1.292 \pm 0.041$	$0.239 \pm 0.005$	$0.064 \pm 0.041$	$8.589 \pm 0.375$	$0.485 \pm 0.007$	$0.494 \pm 0.374$
Nd III	5802	$1.135 \pm 0.032$	$0.088 \pm 0.004$	$0.046 \pm 0.032$	$3.119 \pm 0.221$	$0.381 \pm 0.011$	$0.665 \pm 0.219$
Tb III	5847	$1.359 \pm 0.087$	$0.223 \pm 0.010$	$0.077 \pm 0.086$	$8.381 \pm 0.721$	$0.440 \pm 0.014$	$0.889 \pm 0.730$
Nd III	5851	$1.317 \pm 0.050$	$0.101 \pm 0.006$	$0.087 \pm 0.050$	$4.040 \pm 0.576$	$0.363 \pm 0.022$	$1.101 \pm 0.574$
Tb III	6323	$1.066 \pm 0.074$	$0.224 \pm 0.011$	$0.087 \pm 0.075$	$3.643 \pm 0.436$	$0.479 \pm 0.019$	$0.511 \pm 0.435$
HD 19918, ( $\varphi_{21} - \varphi_{11}$ ) = $0.22 \pm 0.04$							
Pr III	5284	$0.941 \pm 0.041$	$0.056 \pm 0.007$	$0.031 \pm 0.041$	$8.673 \pm 0.352$	$0.238 \pm 0.006$	$0.839 \pm 0.352$
Nd III	5286	$0.951 \pm 0.062$	$0.863 \pm 0.010$	$0.095 \pm 0.062$	$2.306 \pm 0.344$	$0.054 \pm 0.024$	$0.848 \pm 0.340$
Nd III	5294	$0.683 \pm 0.031$	$0.070 \pm 0.007$	$0.047 \pm 0.031$	$7.613 \pm 0.374$	$0.273 \pm 0.008$	$0.353 \pm 0.374$
Pr III	5300	$1.184 \pm 0.054$	$0.061 \pm 0.007$	$0.051 \pm 0.053$	$9.722 \pm 0.547$	$0.285 \pm 0.009$	$0.978 \pm 0.546$
Nd II	5311	$1.087 \pm 0.074$	$0.835 \pm 0.011$	$0.129 \pm 0.073$	$1.863 \pm 0.345$	$0.097 \pm 0.030$	$0.571 \pm 0.343$
Nd II	5319	$1.225 \pm 0.044$	$0.852 \pm 0.006$	$0.140 \pm 0.044$	$2.433 \pm 0.223$	$0.188 \pm 0.014$	$1.133 \pm 0.221$
Nd III	5802	$1.051 \pm 0.032$	$0.927 \pm 0.005$	$0.068 \pm 0.032$	$3.632 \pm 0.219$	$0.216 \pm 0.010$	$1.117 \pm 0.219$
Tb III	5847	$0.887 \pm 0.076$	$0.100 \pm 0.013$	$0.091 \pm 0.075$	$4.390 \pm 0.452$	$0.354 \pm 0.017$	$0.486 \pm 0.456$
Nd III	5851	$1.198 \pm 0.042$	$0.928 \pm 0.006$	$0.062 \pm 0.042$	$4.022 \pm 0.249$	$0.187 \pm 0.010$	$0.968 \pm 0.248$
HD 24712, ( $\varphi_{21} - \varphi_{11}$ ) = $0.19 \pm 0.02$							
Pr III	5284	$0.265 \pm 0.015$	$0.125 \pm 0.009$	$0.001 \pm 0.015$	$0.957 \pm 0.054$	$0.337 \pm 0.009$	$0.045 \pm 0.056$
Nd III	5286	$0.251 \pm 0.011$	$0.833 \pm 0.007$	$0.011 \pm 0.010$	$0.476 \pm 0.045$	$0.962 \pm 0.015$	$0.058 \pm 0.044$
Nd III	5294	$0.176 \pm 0.009$	$0.996 \pm 0.008$	$0.007 \pm 0.009$	$0.343 \pm 0.024$	$0.209 \pm 0.011$	$0.024 \pm 0.024$
Pr III	5300	$0.246 \pm 0.013$	$0.114 \pm 0.009$	$0.006 \pm 0.013$	$0.913 \pm 0.056$	$0.318 \pm 0.010$	$0.039 \pm 0.056$
Nd II	5311	$0.219 \pm 0.009$	$0.821 \pm 0.007$	$0.009 \pm 0.009$	$0.275 \pm 0.032$	$0.987 \pm 0.019$	$0.019 \pm 0.033$
Nd II	5319	$0.245 \pm 0.010$	$0.851 \pm 0.007$	$0.004 \pm 0.010$	$0.280 \pm 0.026$	$0.052 \pm 0.015$	$0.069 \pm 0.027$
Tb III	5505	$0.385 \pm 0.026$	$0.378 \pm 0.011$	$0.009 \pm 0.025$	$1.812 \pm 0.121$	$0.575 \pm 0.011$	$0.121 \pm 0.122$
Tb III	5847	$0.385 \pm 0.027$	$0.348 \pm 0.011$	$0.016 \pm 0.027$	$1.820 \pm 0.189$	$0.508 \pm 0.017$	$0.216 \pm 0.190$
Nd III	5851	$0.243 \pm 0.011$	$0.884 \pm 0.007$	$0.008 \pm 0.011$	$0.556 \pm 0.041$	$0.990 \pm 0.012$	$0.039 \pm 0.041$
HD 101065, ( $\varphi_{21} - \varphi_{11}$ ) = $0.23 \pm 0.02$							
Pr III	5284	$0.441 \pm 0.004$	$0.943 \pm 0.001$	$0.024 \pm 0.004$	$0.258 \pm 0.017$	$0.147 \pm 0.010$	$0.204 \pm 0.017$
Nd III	5286	$0.278 \pm 0.005$	$0.851 \pm 0.003$	$0.015 \pm 0.005$	$0.082 \pm 0.031$	$0.888 \pm 0.059$	$0.113 \pm 0.031$
Nd III	5294	$0.304 \pm 0.004$	$0.897 \pm 0.002$	$0.014 \pm 0.004$	$0.277 \pm 0.023$	$0.876 \pm 0.013$	$0.202 \pm 0.023$
Pr III	5300	$0.460 \pm 0.005$	$0.954 \pm 0.002$	$0.031 \pm 0.005$	$0.628 \pm 0.029$	$0.185 \pm 0.007$	$0.163 \pm 0.029$
Nd II	5311	$0.215 \pm 0.003$	$0.849 \pm 0.002$	$0.009 \pm 0.003$	$0.046 \pm 0.013$	$0.619 \pm 0.047$	$0.114 \pm 0.013$
Nd II	5319	$0.189 \pm 0.002$	$0.857 \pm 0.002$	$0.008 \pm 0.002$	$0.295 \pm 0.009$	$0.356 \pm 0.005$	$0.069 \pm 0.009$
Nd III	5802	$0.218 \pm 0.004$	$0.855 \pm 0.003$	$0.011 \pm 0.004$	$0.227 \pm 0.014$	$0.833 \pm 0.009$	$0.098 \pm 0.014$
Tb III	5847	$0.704 \pm 0.013$	$0.111 \pm 0.003$	$0.028 \pm 0.013$	$3.588 \pm 0.128$	$0.360 \pm 0.006$	$0.089 \pm 0.128$
Nd III	5851	$0.239 \pm 0.005$	$0.847 \pm 0.003$	$0.013 \pm 0.005$	$0.281 \pm 0.024$	$0.822 \pm 0.013$	$0.166 \pm 0.023$
Tb III	6323	$0.646 \pm 0.015$	$0.107 \pm 0.004$	$0.037 \pm 0.015$	$2.856 \pm 0.124$	$0.337 \pm 0.007$	$0.087 \pm 0.123$

the middle of the expansion part of the radius phase curve. At the maximum radius, RV returns to zero. Then the positive part of the RV curve describes contraction phase, and radius reaches minimum when  $\langle V \rangle$  returns to zero after positive extremum. Adding

to this picture the  $\langle V^2 \rangle$  variability discussed above, we find that linewidth changes approximately in antiphase (i.e. with a phase shift of 0.5) with respect to stellar radius variation. In other words, the maximum contraction (minimum radius) phase point corresponds

**Table 4.** Results of the least-squares fitting of the first and second moment variation of the REE lines in HD 122970, HD 128898, HD 134214 and HD 137949. See caption of Table 3 for the explanation of this table's content.

Ion	$\lambda$ (Å)	$V_{11}$ (km s <sup>-1</sup> )	$\langle V \rangle$ $\varphi_{11}$	$V_{12}$ (km s <sup>-1</sup> )	$V_{21}$ (km <sup>2</sup> s <sup>-2</sup> )	$\langle V^2 \rangle$ $\varphi_{21}$	$V_{22}$ (km <sup>2</sup> s <sup>-2</sup> )
HD 122970, ( $\varphi_{21} - \varphi_{11}$ ) = 0.22 ± 0.04							
Pr III	5284	0.614 ± 0.016	0.891 ± 0.004	0.032 ± 0.016	0.930 ± 0.068	0.926 ± 0.012	0.465 ± 0.068
Nd III	5286	0.535 ± 0.027	0.844 ± 0.008	0.021 ± 0.027	0.309 ± 0.120	0.729 ± 0.063	0.227 ± 0.121
Nd III	5294	0.434 ± 0.011	0.853 ± 0.004	0.025 ± 0.011	0.270 ± 0.040	0.875 ± 0.024	0.118 ± 0.040
Pr III	5300	0.586 ± 0.014	0.886 ± 0.004	0.020 ± 0.014	0.283 ± 0.058	0.086 ± 0.033	0.245 ± 0.058
Nd II	5311	0.490 ± 0.023	0.842 ± 0.007	0.028 ± 0.023	0.103 ± 0.101	0.828 ± 0.154	0.154 ± 0.101
Nd II	5319	0.430 ± 0.012	0.843 ± 0.005	0.006 ± 0.012	0.074 ± 0.041	0.206 ± 0.089	0.163 ± 0.041
Tb III	5505	1.107 ± 0.026	0.953 ± 0.004	0.136 ± 0.026	1.504 ± 0.146	0.213 ± 0.015	0.838 ± 0.145
Nd III	5802	0.511 ± 0.020	0.846 ± 0.006	0.019 ± 0.020	0.126 ± 0.085	0.953 ± 0.108	0.143 ± 0.085
Tb III	5847	1.095 ± 0.039	0.930 ± 0.006	0.113 ± 0.038	1.383 ± 0.210	0.113 ± 0.024	1.185 ± 0.211
Nd III	5851	0.515 ± 0.019	0.853 ± 0.006	0.030 ± 0.019	0.553 ± 0.096	0.948 ± 0.028	0.422 ± 0.096
Tb III	6323	1.197 ± 0.053	0.946 ± 0.007	0.169 ± 0.052	1.239 ± 0.320	0.176 ± 0.041	1.096 ± 0.315
HD 128898, ( $\varphi_{21} - \varphi_{11}$ ) = 0.28 ± 0.04							
Pr III	5284	0.509 ± 0.011	0.670 ± 0.003	0.017 ± 0.011	2.715 ± 0.084	0.887 ± 0.005	0.046 ± 0.084
Nd III	5286	0.708 ± 0.018	0.359 ± 0.004	0.075 ± 0.018	2.248 ± 0.132	0.687 ± 0.009	0.346 ± 0.132
Nd III	5294	0.287 ± 0.009	0.604 ± 0.005	0.025 ± 0.009	1.740 ± 0.080	0.911 ± 0.007	0.002 ± 0.080
Pr III	5300	0.513 ± 0.012	0.660 ± 0.004	0.020 ± 0.012	2.916 ± 0.100	0.937 ± 0.005	0.133 ± 0.099
Nd II	5319	0.815 ± 0.018	0.333 ± 0.003	0.067 ± 0.018	2.553 ± 0.132	0.778 ± 0.008	0.289 ± 0.131
Tb III	5505	0.777 ± 0.017	0.840 ± 0.003	0.059 ± 0.017	5.088 ± 0.153	0.137 ± 0.005	0.014 ± 0.154
Nd III	5802	0.512 ± 0.013	0.432 ± 0.004	0.036 ± 0.013	1.930 ± 0.110	0.798 ± 0.009	0.236 ± 0.110
Tb III	5847	0.854 ± 0.033	0.834 ± 0.006	0.076 ± 0.033	5.376 ± 0.257	0.123 ± 0.008	0.295 ± 0.257
Nd III	5851	0.563 ± 0.014	0.441 ± 0.004	0.046 ± 0.014	2.088 ± 0.105	0.769 ± 0.008	0.431 ± 0.105
Tb III	6323	0.746 ± 0.040	0.802 ± 0.008	0.055 ± 0.040	3.781 ± 0.271	0.108 ± 0.011	0.612 ± 0.270
HD 134214, ( $\varphi_{21} - \varphi_{11}$ ) = 0.20 ± 0.03							
Pr III	5284	0.387 ± 0.016	0.226 ± 0.007	0.010 ± 0.016	2.241 ± 0.102	0.376 ± 0.007	0.063 ± 0.103
Nd III	5286	0.553 ± 0.021	0.921 ± 0.006	0.014 ± 0.021	1.233 ± 0.127	0.099 ± 0.016	0.100 ± 0.128
Nd III	5294	0.207 ± 0.010	0.095 ± 0.007	0.010 ± 0.010	0.728 ± 0.052	0.374 ± 0.011	0.052 ± 0.052
Pr III	5300	0.362 ± 0.015	0.205 ± 0.006	0.013 ± 0.015	2.266 ± 0.104	0.425 ± 0.007	0.122 ± 0.104
Nd II	5311	0.508 ± 0.019	0.894 ± 0.006	0.001 ± 0.020	0.482 ± 0.073	0.120 ± 0.024	0.242 ± 0.072
Nd II	5319	0.522 ± 0.018	0.928 ± 0.006	0.010 ± 0.018	0.843 ± 0.053	0.214 ± 0.010	0.155 ± 0.053
Tb III	5505	0.508 ± 0.027	0.410 ± 0.009	0.026 ± 0.027	2.713 ± 0.159	0.614 ± 0.009	0.143 ± 0.158
Nd III	5802	0.444 ± 0.018	0.963 ± 0.006	0.004 ± 0.018	1.137 ± 0.085	0.155 ± 0.012	0.137 ± 0.085
Tb III	5847	0.549 ± 0.043	0.395 ± 0.013	0.017 ± 0.043	4.243 ± 0.375	0.613 ± 0.014	0.513 ± 0.377
Nd III	5851	0.490 ± 0.019	0.964 ± 0.006	0.019 ± 0.019	1.308 ± 0.098	0.179 ± 0.012	0.116 ± 0.099
Tb III	6323	0.673 ± 0.060	0.413 ± 0.014	0.045 ± 0.059	3.683 ± 0.546	0.606 ± 0.023	0.527 ± 0.549
HD 137949, ( $\varphi_{21} - \varphi_{11}$ ) = 0.27 ± 0.07							
Pr III	5284	0.056 ± 0.004	0.307 ± 0.010	0.028 ± 0.004	0.535 ± 0.027	0.500 ± 0.008	0.242 ± 0.027
Nd III	5286	0.023 ± 0.005	0.723 ± 0.036	0.059 ± 0.005	0.383 ± 0.060	0.246 ± 0.025	0.588 ± 0.059
Nd III	5294	0.128 ± 0.006	0.336 ± 0.007	0.011 ± 0.006	0.779 ± 0.064	0.582 ± 0.013	0.246 ± 0.064
Pr III	5300	0.069 ± 0.005	0.253 ± 0.011	0.035 ± 0.005	0.576 ± 0.044	0.492 ± 0.012	0.293 ± 0.044
Nd II	5311	0.096 ± 0.005	0.715 ± 0.007	0.047 ± 0.005	0.135 ± 0.020	0.966 ± 0.024	0.499 ± 0.020
Nd II	5319	0.114 ± 0.005	0.795 ± 0.008	0.066 ± 0.005	0.157 ± 0.034	0.184 ± 0.035	0.642 ± 0.034
Nd III	5802	0.064 ± 0.006	0.298 ± 0.016	0.042 ± 0.006	0.585 ± 0.065	0.330 ± 0.018	0.228 ± 0.065
Tb III	5847	0.096 ± 0.009	0.003 ± 0.015	0.062 ± 0.009	0.268 ± 0.072	0.355 ± 0.043	0.587 ± 0.072
Nd III	5851	0.064 ± 0.008	0.244 ± 0.020	0.070 ± 0.008	0.604 ± 0.103	0.443 ± 0.027	0.532 ± 0.103
Tb III	6323	0.175 ± 0.017	0.051 ± 0.016	0.099 ± 0.017	0.971 ± 0.169	0.357 ± 0.028	0.929 ± 0.169

to maximum linewidth, whereas at the phase of maximum expansion (maximum radius) lines become narrower. This fundamental relation between pulsational modulation of linewidth on the one hand and RV and radius changes on the other hand is sketched in Fig. 10.

The tendency of REE lines to become broader at the maximum contraction phase is confirmed by investigation of the time-resolved spectra of  $\gamma$  Equ. As was already mentioned above, our 2001 CFHT observations caught this star in a remarkably high-amplitude pulsation state. The very high  $S/N$  and high resolution of these data reveal pulsational profile variation synchronized with radius changes. Fig. 11 compares the average profile of the Nd III 6550 Å line with

the time-resolved spectra corresponding to nearly zero RV, but different extrema of the  $\langle V^2 \rangle$  phase curve. Time-resolved spectra for the minimum and maximum  $\langle V^2 \rangle$  exhibit different width, yet the equivalent width of the line does not change appreciably. This evidence confirms that our measurements of the second moment of REE in roAp stars diagnose pulsational perturbation of linewidth, not some other unrecognized line profile or line strength fluctuations.

#### 4.4 Short-term variation of moment amplitudes

Kochukhov & Ryabchikova (2001b) discovered that the amplitude of the pulsational RV variability of the Nd III 6145 Å line in  $\alpha$  Cir

**Table 5.** Results of the least-squares fitting of the first and second moment variation of the REE lines in HD 201601. See caption of Table 3 for the explanation of this table's content. The phase difference  $\varphi_{21} - \varphi_{11}$  is obtained using the lines of Pr III, Nd III and Tb III.

Ion	$\lambda$ (Å)	$V_{11}$ (km s <sup>-1</sup> )	$\langle V \rangle$ $\varphi_{11}$	$V_{12}$ (km s <sup>-1</sup> )	$V_{21}$ (km <sup>2</sup> s <sup>-2</sup> )	$\langle V^2 \rangle$ $\varphi_{21}$	$V_{22}$ (km <sup>2</sup> s <sup>-2</sup> )
HD 201601 <sup>1</sup> , $\langle \varphi_{21} - \varphi_{11} \rangle = 0.21$							
Nd III	6145	0.458 ± 0.016	0.178 ± 0.005	0.056 ± 0.016	2.989 ± 0.186	0.390 ± 0.010	0.574 ± 0.194
Pr III	6160	0.642 ± 0.018	0.179 ± 0.004	0.067 ± 0.019	3.192 ± 0.183	0.385 ± 0.009	0.302 ± 0.188
HD 201601 <sup>2</sup> , $\langle \varphi_{21} - \varphi_{11} \rangle = 0.26 \pm 0.05$							
Nd III	6550	0.737 ± 0.011	0.605 ± 0.002	0.060 ± 0.011	5.038 ± 0.248	0.836 ± 0.008	0.066 ± 0.246
Nd II	6650	1.131 ± 0.021	0.399 ± 0.003	0.130 ± 0.020	2.063 ± 0.178	0.607 ± 0.014	0.969 ± 0.177
Nd III	6691	1.078 ± 0.020	0.509 ± 0.003	0.097 ± 0.020	2.792 ± 0.280	0.791 ± 0.016	1.193 ± 0.276
Pr III	6706	0.841 ± 0.027	0.599 ± 0.005	0.070 ± 0.027	4.495 ± 0.392	0.901 ± 0.014	1.081 ± 0.393
HD 201601 <sup>3</sup> , $\langle \varphi_{21} - \varphi_{11} \rangle = 0.26 \pm 0.06$							
Pr III	5284	0.158 ± 0.006	0.345 ± 0.006	0.007 ± 0.006	0.405 ± 0.064	0.581 ± 0.025	0.075 ± 0.064
Nd III	5286	0.319 ± 0.013	0.185 ± 0.007	0.011 ± 0.013	0.714 ± 0.144	0.431 ± 0.032	0.079 ± 0.143
Nd III	5294	0.104 ± 0.007	0.372 ± 0.011	0.002 ± 0.007	0.791 ± 0.067	0.564 ± 0.014	0.101 ± 0.068
Pr III	5300	0.234 ± 0.010	0.346 ± 0.006	0.025 ± 0.010	1.094 ± 0.114	0.577 ± 0.017	0.152 ± 0.116
Nd II	5311	0.277 ± 0.013	0.139 ± 0.008	0.032 ± 0.013	0.253 ± 0.056	0.473 ± 0.036	0.085 ± 0.056
Nd II	5319	0.310 ± 0.010	0.178 ± 0.005	0.018 ± 0.010	0.303 ± 0.042	0.465 ± 0.022	0.095 ± 0.042
Tb III	5847	0.222 ± 0.038	0.499 ± 0.028	0.071 ± 0.038	1.193 ± 0.349	0.851 ± 0.047	0.268 ± 0.353
Nd III	5851	0.218 ± 0.016	0.375 ± 0.012	0.028 ± 0.016	0.667 ± 0.130	0.661 ± 0.031	0.290 ± 0.129
HD 201601 <sup>4</sup> , $\langle \varphi_{21} - \varphi_{11} \rangle = 0.15$							
Tb III	5847	0.178 ± 0.046	0.823 ± 0.041	0.034 ± 0.046	1.318 ± 0.489	0.997 ± 0.059	0.440 ± 0.481
Nd III	5851	0.199 ± 0.016	0.705 ± 0.013	0.012 ± 0.016	0.515 ± 0.144	0.838 ± 0.044	0.250 ± 0.144
HD 201601 <sup>5</sup> , $\langle \varphi_{21} - \varphi_{11} \rangle = 0.25$							
Nd III	6550	0.118 ± 0.013	0.906 ± 0.017	0.002 ± 0.013	0.579 ± 0.167	0.182 ± 0.046	0.231 ± 0.165
Nd II	6650	0.149 ± 0.028	0.715 ± 0.031	0.015 ± 0.029	0.214 ± 0.166	0.933 ± 0.123	0.173 ± 0.166
HD 201601 <sup>6</sup> , $\langle \varphi_{21} - \varphi_{11} \rangle = 0.23$							
Nd III	6145	0.155 ± 0.008	0.521 ± 0.008	0.013 ± 0.008	0.843 ± 0.148	0.751 ± 0.028	0.102 ± 0.147
Pr III	6160	0.175 ± 0.011	0.546 ± 0.010	0.025 ± 0.011	0.910 ± 0.082	0.783 ± 0.014	0.188 ± 0.081

(HD 128898) changes significantly within a time period of about one hour. This modulation of RV oscillations occurs on a time-scale much shorter than the 4.471 d rotation period of  $\alpha$  Cir and cannot be ascribed to beating between known close frequencies because photometric studies (Kurtz et al. 1994) show that this roAp star is essentially a monoprotic pulsator. In a recent investigation of the pulsational RV variability of Pr III lines, Kurtz et al. (2006) confirmed the presence of short-term changes of RV amplitude in  $\alpha$  Cir and demonstrated the existence of similar behaviour in a few other roAp stars. Among various possible explanations for the new spectroscopic frequencies, observed in Pr III but absent in broadband photometry, Kurtz et al. (2006) favoured the idea that at the formation heights of Pr III lines the pulsational RV amplitude experiences stochastic variation due to growth and decay of the principal pulsation mode.

We have performed a new analysis of the short-term changes of pulsational variability using time series of both the first and the second moments measured in the UVES time-resolved spectra of  $\alpha$  Cir. We explored the behaviour of several REE ions (Pr III, Nd II, Nd III, Tb III) and considered the results in the light of the newly discovered depth dependence of the pulsational LPV pattern and linewidth oscillations. Analysis of the amplitude variability for the REE line profile moments was based on the least-squares fitting introduced in Section 4.3, except that here we adjust amplitude and phase for the principal frequency ( $P_1 = 6.80$  min) and a secondary periodicity  $P_2 = 7.34$  min (Kurtz et al. 2006), responsible for the observed short-term modulation. The strength of the amplitude modulation is then characterized by the respective amplitude ratio  $V_2/V_1$ , estimated separately for the first and second moments.

Numerical results of the least-squares analysis of the moment time series are summarized in Table 6 for nine REE lines. Clearly, we find different amounts of RV amplitude modulation for different REE ions. The secondary frequency is at the detection threshold for the Nd II 5319 Å line. The  $V_2/V_1$  amplitude ratio increases by a factor of 2–3 towards the higher atmospheric layers where doubly ionized REE lines are formed. This is further illustrated in Fig. 12, where we show the observed and best-fitting RV curve for the Nd II 5319 Å and Tb III 5505 Å lines. One can clearly see that pulsations in the latter line change appreciably with time, whereas much weaker modulation is observed for the former line. This figure and Table 6 provides the first definite demonstration of the height variation of the short-term amplitude modulation effect in  $\alpha$  Cir. Moreover, time-series analysis of the second moment reveals a much stronger (by a factor of 1.5–3) amplitude modulation compared to the RV results. This is unexpected because the relative amplitudes of the two frequencies should be the same for both  $\langle V \rangle$  and  $\langle V^2 \rangle$  (Mathias et al. 1994).

Thus, it is tempting to speculate that, whatever effect gives rise to the observed RV amplitude variability in the upper atmosphere of  $\alpha$  Cir, it acts more strongly on the linewidth variation than on the first moment. Considering these results in the light of our discovery of the steep growth of the linewidth oscillations with height, we suggest that the observed short-term modulation is actually a property of the physical mechanism responsible for the linewidth and asymmetric LPV behaviour, while the short-term amplitude changes visible in RV represent a secondary consequence of the action of this hypothetical mechanism. Further investigation of several roAp stars is required to verify this hypothesis. In particular, a full

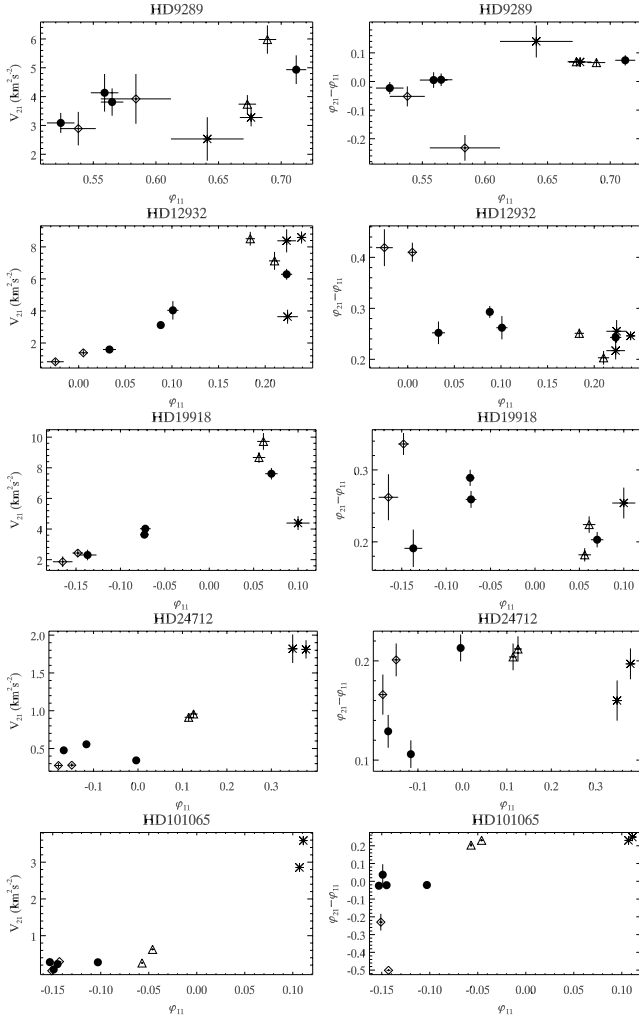


**Figure 8.** The amplitude  $V_{21}$  of the second moment variation at the main frequency (left-hand panels) and the phase difference  $\varphi_{21} - \varphi_{11}$  (right-hand panels) as a function of the pulsation phase  $\varphi_{11}$  of RV changes for HD 9289, HD 12932, HD 19918, HD 24712 and HD 101065. Symbols correspond to different REE ions: Pr III ( $\Delta$ ), Nd II ( $\diamond$ ), Nd III ( $\bullet$ ), Tb III ( $*$ ).

night of uninterrupted time-resolved monitoring of  $\alpha$  Cir would be extremely useful to discriminate between a truly stochastic and a quasi-periodic nature of the variation of oscillation amplitudes in the upper atmospheric layers.

## 5 INTERPRETATION

Our survey of the pulsational line profile variability in sharp-lined roAp stars has revealed a new type of LPV behaviour and has demonstrated its significant depth dependence. In summary, our observational findings are as follows.

(i) The asymmetric, blue-to-red wave pattern is common in time-resolved residual spectra of roAp stars. This behaviour is more pronounced for REE lines formed in the higher atmospheric layers, whereas lines originating at the bottom of the REE-enriched cloud often display S-shaped, symmetric, blue-to-red-to-blue LPV pattern.

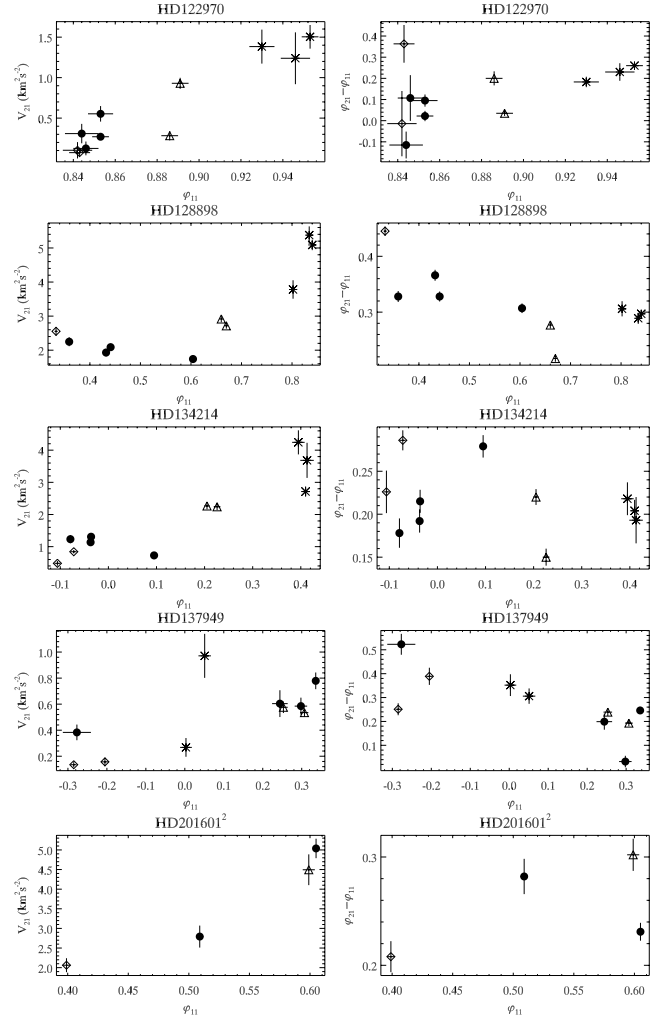


**Figure 9.** Same as Fig. 8 for HD 122970, HD 128898, HD 134214, HD 137949 and HD 201601.

(ii) The doubly ionized REE lines from the uppermost part of the stellar atmosphere show strong single-wave pulsational variability of linewidth. These oscillations typically occur in antiphase with the pulsational changes of stellar radius. They also correlate with the presence of asymmetric LPV and exhibit the same height dependence.

(iii) The efficiency of the mechanism responsible for the asymmetric LPV pattern and single-wave linewidth variation in HD 128898 changes on relatively short time-scales.

These results, in particular the new type of pulsational LPV described by (i) and (ii), challenge our understanding of pulsations in roAp stars and call for theoretical explanation. In this section we present a series of line profile calculations for oblique non-radial pulsations and compare observations with theoretical expectations. We show that the standard models including only spherical harmonic perturbations of velocity fail to reproduce the observed line profile and moment variability. This led us to introduce a new OPM, which accounts for additional linewidth oscillations. Using this new modelling framework, we are able to explain all the main characteristics of the pulsational LPV in sharp-lined roAp stars.

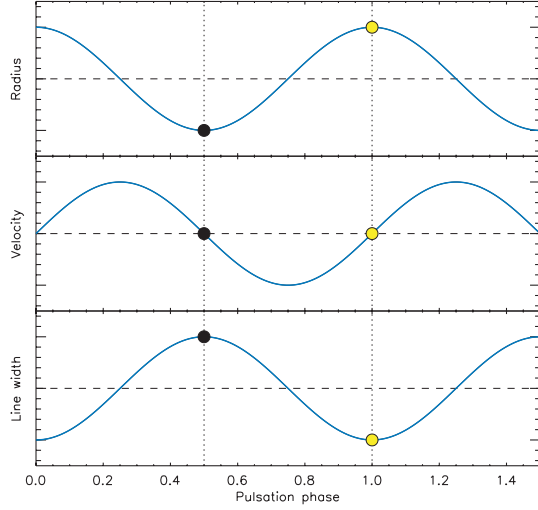


**Figure 10.** Illustration of the phase relation between pulsational modulation of stellar radius, RV and linewidth discovered in our study. Symbols mark the phase point of maximum compression (filled circle) and maximum expansion (open circle).

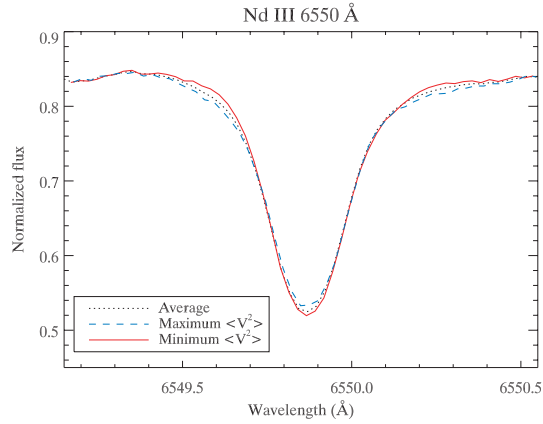


**Figure 11.** Linewidth variation for the Nd III 6550 Å line in the spectrum of  $\gamma$  Equ. The average profile (dotted curve) is compared with the time-resolved spectra corresponding to minimum (solid curve) and maximum (dashed curve) of the second moment.

### 5.1 Spectrum synthesis calculations for oblique pulsators

Periodic variation of velocity in non-radial pulsators is described with the spherical harmonics  $Y_\ell^m(\theta, \phi)$  and their derivatives:

$$\begin{aligned} V_r &= V_p Y_\ell^m(\theta, \phi) e^{i\omega t}, \\ V_\theta &= K V_p \frac{\partial}{\partial \theta} Y_\ell^m(\theta, \phi) e^{i\omega t}, \\ V_\phi &= K V_p \frac{1}{\sin \theta} \frac{\partial}{\partial \phi} Y_\ell^m(\theta, \phi) e^{i\omega t}, \end{aligned} \quad (3)$$

where  $\omega$  is the angular pulsation frequency,  $V_p$  is the pulsation amplitude and  $K$  is the ratio of the vertical to horizontal amplitudes. Non-radial oscillations in roAp stars are oblique. Therefore, spherical angular coordinates  $\theta$ ,  $\phi$  refer to a reference system whose orientation is defined by the angles  $\beta$  and  $\chi$  with respect to the stellar axis of rotation. In the classical OPM, the pulsation axis is assumed to be aligned with the axis of a quasi-dipolar magnetic

**Table 6.** Amplitude modulation for the oscillations in the first and second moments of REE lines in  $\alpha$  Cir. The columns give line identification and the amplitude ratio  $V_2/V_1$ , which characterizes the strength of the secondary periodicity ( $P_2 = 7.34$  min) with respect to the amplitude of the principal frequency ( $P_1 = 6.80$  min).

Ion	$\lambda$ (Å)	$\langle V \rangle$	$V_2/V_1$ $\langle V^2 \rangle$
Pr III	5284	$0.192 \pm 0.018$	$0.331 \pm 0.026$
Nd III	5286	$0.154 \pm 0.025$	$0.392 \pm 0.062$
Nd III	5294	$0.255 \pm 0.031$	$0.360 \pm 0.046$
Pr III	5300	$0.165 \pm 0.022$	$0.369 \pm 0.029$
Nd II	5319	$0.073 \pm 0.022$	$0.224 \pm 0.053$
Tb III	5505	$0.220 \pm 0.018$	$0.371 \pm 0.023$
Nd III	5802	$0.141 \pm 0.024$	$0.423 \pm 0.059$
Tb III	5847	$0.188 \pm 0.038$	$0.334 \pm 0.050$
Nd III	5851	$0.198 \pm 0.024$	$0.370 \pm 0.054$

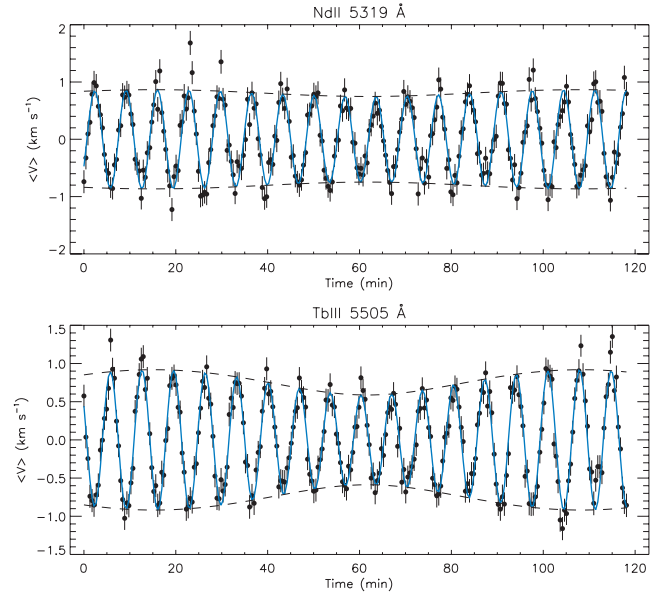


**Figure 12.** Modulation of RV amplitude for the Nd II 5319 Å (upper panel) and Tb III 5505 Å (lower panel) lines in HD 128898. Symbols show velocity measurements, solid line corresponds to the best-fitting superposition of the variability with  $P_1 = 6.80$  min and  $P_2 = 7.34$  min. The dashed curve illustrates temporal variation of the principal frequency amplitude.

field. In this case,  $\theta$  and  $\phi$  are spherical angular coordinates in the magnetic reference frame.

Equation (3) can easily be generalized (see Kochukhov 2004a) for the situation when pulsation modes are distorted by stellar rotation and/or a strong magnetic field and are described by superposition of several spherical harmonic functions.

The horizontal to vertical amplitude ratio is usually approximated as

$$K = \frac{GM}{\omega^2 R^3} \quad (4)$$

(e.g. Smeyers & Tassoul 1987). This relation predicts that vertical oscillations should be dominant (i.e.  $K \ll 1$ ) for high-overtone p modes in roAp stars. Consequently, horizontal displacement was often neglected in previous studies of roAp pulsations (Bigot & Dziembowski 2002). However, the distorted magnetoacoustic

pulsations modes in the theory of Saio & Gautschy (2004) show significant horizontal amplitudes ( $K \sim 1$ ) in the lower part of stellar atmosphere.

For the purpose of computing theoretical LPV, the pulsation velocity field described by equation (3) is transformed to the Descartes coordinate system of the observer. The line-of-sight velocity component,  $V^o$ , which enters spectrum synthesis, combines the contribution of pulsations and the Doppler shift due to solid body stellar rotation with the projected rotational velocity  $v_e \sin i$ . For the sake of brevity here we omit details of coordinate transformations, definition of spherical harmonics and calculation of their derivatives. Interested readers can find this information in Kochukhov (2004a, 2005).

Even neglecting possible rotational and magnetic distortion of the non-radial pulsations, the model formulated above has a large number of free parameters. One has to specify the amplitude and structure of the pulsation mode,  $V_p, K, \ell, m$ , as well as the orientation of the pulsation axis  $\beta, \chi$ , and the stellar  $v_e \sin i$  and inclination angle  $i$ . In the limit of negligible  $v_e \sin i$  applicable to many roAp stars, the angles  $\beta, \chi$  and  $i$  can be replaced by a single parameter  $\alpha$  – the angle between the line of sight and pulsation axis.

In order to be able to explore properties of LPV for many different pulsation geometries in a reasonable amount of time, we approximate the local line profile with a Gaussian function, characterized by a constant central depth  $D$  and full width at half maximum  $W$ . Then the disc-integrated line profile  $S$  is obtained by the weighted summation over all visible surface zones

$$S = 1 - D \sum_{j=1}^N T_j e^{-4 \ln 2 \frac{(v - V^o)^2}{W^2}}, \quad (5)$$

where the weight function

$$T_j = \frac{3(1 - u + u\mu_j)\mu_j A_j}{\pi(3 - u)} \quad (6)$$

accounts for unequal projected areas of surface elements and includes a linear limb-darkening law with coefficient  $u$ , and  $\mu$  denotes the cosine of the angle between the line of sight and the surface normal. In all simulations described below, we use  $D = 0.5, W =$

$10 \text{ km s}^{-1}, u = 0.5$ .  $V_p$  and  $K$  are chosen in such a way that the resultant RV amplitude is compatible with the one typically found in roAp stars ( $\sim 1 \text{ km s}^{-1}$ ). The stellar surface is sampled on a 3909-element grid with unequal number of surface zones at different latitudes (see Piskunov & Kochukhov 2002). Calculations are performed for a set of 20 equally spaced pulsation phases. Equation (1) is used to infer variation of the first and second moments from theoretical line profile time series.

Our LPV synthesis model is very similar to the one usually used in a broader context of spectral variability studies of non-radial pulsations in slowly rotating stars (Aerts & Waelkens 1993; Schrijvers et al. 1997). Using this standard description of oscillations and accounting for the additional complication caused by oblique mode geometry, we carried out an extensive set of computations aiming to find a combination of input parameters that produces LPV compatible with observations. Pulsational LPV and moment variability was investigated for

- (i) all possible modes with  $\ell \leq 3$ ;
- (ii) projected rotational velocities in the range  $0\text{--}10 \text{ km s}^{-1}$ ;
- (iii) modes with significant ( $K \sim 1$ ) and dominant ( $K \gg 1$ ) horizontal fluctuations;
- (iv) distorted dipolar modes given by superposition of  $\ell = 1, m = -1, 0, 1$  spherical harmonics (Bigot & Dziembowski 2002) or by superposition of  $\ell = 1$  and  $\ell = 3$  axisymmetric harmonics (Saio & Gautschy 2004);
- (v) modes containing two pulsation components with different  $K$  and a phase shift relative to each other – this model is meant to simulate superposition of magnetic and acoustic running wave components possibly existing in the upper atmospheres of roAp stars (Cunha 2006).

We found that none of the pulsation structures studied leads to a qualitative agreement with observations. A typical failure of the theoretical model is illustrated in Fig. 13(a) for the  $\ell = 1, m = 0$  mode viewed from the pulsation pole. The residual profile variation has a symmetric S-shape and the linewidth changes have low-amplitude, double-wave character. In the absence of stellar rotation, LPV for all pulsation modes have these basic properties – the same

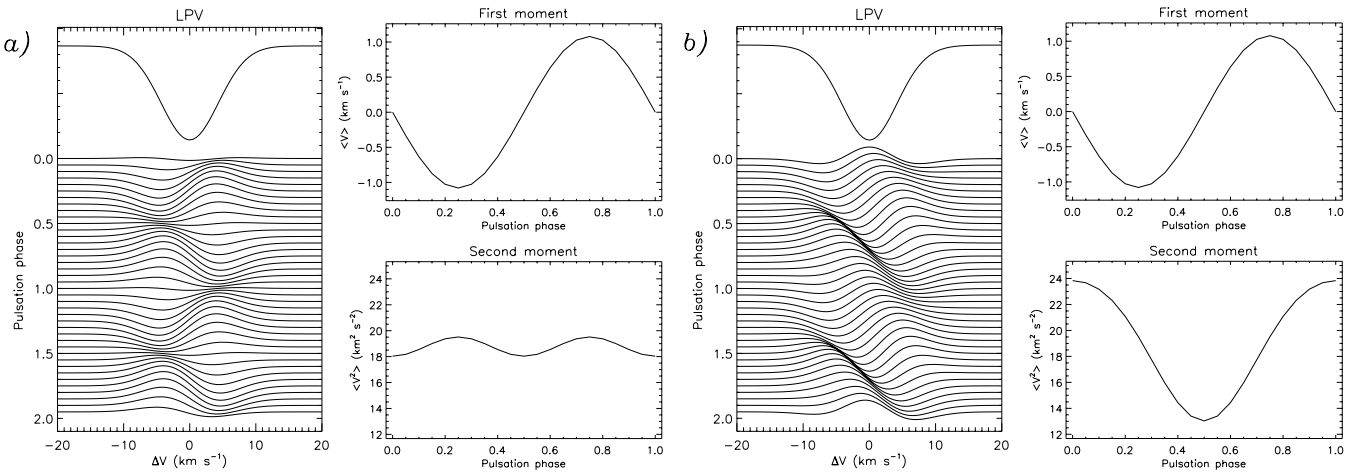


**Figure 13.** LPV of a non-rotating non-radial pulsator. (a) Spectrum variability for the  $\ell = 1, m = 0, V_p = 2.0 \text{ km s}^{-1}, K = 0$  mode viewed from the pulsation pole. The local profile is represented by a constant Gaussian with FWHM  $W = 10 \text{ km s}^{-1}$ . (b) Effect of adding harmonic variability of the linewidth with an amplitude  $\delta W = 1.5 \text{ km s}^{-1}$  and a phase shift of 0.25 with respect to the pulsational velocity variation. In both cases, the star is assumed to have  $v_e \sin i = 0 \text{ km s}^{-1}$ . In each panel the left-hand plot shows the average line profile on top and time series of the difference spectra (covering two pulsation cycles) below. The right-hand panels illustrate variation of the first (upper plot) and second (lower plot) line profile moments.

conclusion follows from the theoretical analysis of the second moment behaviour (Aerts et al. 1992; Kochukhov 2005). This variability is not incompatible with observations of weak Nd II lines in a few roAp stars, but clearly contradicts pulsation signatures found for the majority of doubly ionized REE lines.

When significant ( $v_e \sin i \gg V_p$ ) rotational velocity is introduced in the model and the pulsation pole of the dipolar mode is offset from the line of sight, one may encounter LPV characterized by significant single-wave linewidth changes. However, the phase shift of RV and linewidth oscillations is inconsistent with observations. Moreover, for this pulsational geometry a small RV amplitude corresponds to a quite strong LPV, which has a fully symmetric (both in time and relative to the line centre) H-shape and thus appears to be very different from the observed blue-to-red residual profile shift.

Our calculations show that all types of complex modes, obtained by combining different spherical harmonics or by combining components with different phase shifts, also fail to achieve a satisfactory agreement with observations. The key features of the roAp line profile behaviour – single-wave linewidth oscillations with a characteristic phase shift and asymmetric LPV pattern – are never found for the theoretical models explored. Thus, we conclude that the standard picture of the velocity field in non-radial pulsators and trivial extensions of this picture are inadequate for the REE lines which form in the upper atmospheres and show the most prominent pulsation signatures in roAp stars.

Admittedly, the simplified line formation model adopted in our calculations does not allow one to properly explore effects of the depth dependent pulsation amplitude and phase. However, we expect that any superposition of several harmonic oscillations will give another harmonic oscillation. Consequently, variation of the pulsation wave properties with height will not introduce any qualitatively new behaviour and will not help to explain the puzzling spectroscopic observations of roAp stars.

It appears that the key problem lies in the formulation of the standard pulsation framework: the time-dependent factor in equation (3) postulates symmetry of the compression and expansion parts of pulsation cycle. In reality the opposite, asymmetric behaviour is observed in roAp stars (see Section 4 and Fig. 10).

## 5.2 A new OPM

We have discovered that the enigma of LPV in roAp stars can be resolved with a simple modification of the classical oblique pulsator framework. Instead of looking for a combination of pulsation parameters which gives the variation of the disc-integrated quantities illustrated in Fig. 10, we suggest that this empirical relation between radius, RV and second moment changes actually reflects a *local* periodic variation of velocity and linewidth. Thus, the key idea of our new OPM is that the pulsational mechanism responsible for the RV variability of REE lines gives rise to additional, sinusoidal changes of linewidth. This variability occurs approximately in antiphase with the pulsational radius changes and hence shows a quarter of period phase shift with respect to RV oscillations. Then the LPV expected from this model is a combination of two effects:

- (i) the usual pulsational velocity changes described by spherical harmonic perturbations and
- (ii) sinusoidal variability of line profile width, synchronized with changes of stellar radius.

It is reasonable to assume that the surface distribution of the linewidth amplitude is similar to the vertical pulsational displace-

ment and is described by

$$W(t, \theta, \phi) = W_0 + \delta W Y_\ell^m(\theta, \phi) e^{i(\omega t - \varphi_W)}. \quad (7)$$

The theoretical LPV can be calculated by incorporating this time and position-dependent linewidth in the disc-integration formula (5). A striking effect of introducing variable linewidth in the line profile synthesis is demonstrated by Fig. 13(b). The pulsation model used for this figure is identical to the model of Fig. 13(a), except that now linewidth changes with an amplitude  $\delta W = 1.5 \text{ km s}^{-1}$  around  $W_0 = 10 \text{ km s}^{-1}$  and a phase shift  $\varphi_W = 0.25$ . This leads to a remarkable agreement between theoretical residual profile variation and observations of roAp stars. Model spectra show smooth, blue-to-red moving pattern, which is very similar to the LPV discussed in Section 4.2. The additional variation of linewidth does not distort the sinusoidal behaviour of the RV. Considering the second moment oscillations, we find that a large-amplitude single-wave variability superimposed on top of a small-amplitude double-wave curve results in nearly sinusoidal variation of  $\langle V^2 \rangle$ . The phase shift assumed for the time dependence of the local velocity and linewidth propagates to the disc-integrated observables, allowing us to reproduce the observed phase lag of  $\langle V^2 \rangle$  with respect to  $\langle V \rangle$ .

An interesting modification of the LPV pattern calculated with our model is associated with increasing  $v_e \sin i$ . The LPV corresponding to  $v_e \sin i = 0 \text{ km s}^{-1}$  is presented in Fig. 13(b). Figs 14(a) and (b) show LPV for the same oblique pulsator geometry and amplitude, but with  $v_e \sin i$  increased to 10 and 20  $\text{km s}^{-1}$ , respectively. The blue-to-red shift is still discernible for the  $v_e \sin i = 10 \text{ km s}^{-1}$  model, although it is not as smooth as in non-rotating star. In the case of rapid rotation (Fig. 14b), the signature of linewidth variability disappears and the LPV shows an almost symmetric pattern, as one would expect for the standard oblique pulsator. Thus, if the  $\delta W$  amplitude adopted for these simulations is realistic, we predict that a signature of the pulsational variation of linewidth will be visible only in slowly rotating stars ( $v_e \sin i \lesssim 10 \text{ km s}^{-1}$ ), but not in relatively rapid rotators ( $v_e \sin i \gtrsim 20 \text{ km s}^{-1}$ ). In fact, this prediction is verified by observations. We find asymmetric LPV in all slowly rotating roAp stars, including HD 9289 and HD 128898 ( $v_e \sin i \sim 10 \text{ km s}^{-1}$ ), whereas the study of high-amplitude, rapidly rotating ( $v_e \sin i = 33 \text{ km s}^{-1}$ ) roAp pulsator HD 83368 reveals a symmetric LPV pattern and no evidence of blue-to-red shifting features in residual line profiles (Kochukhov 2006).

We have performed additional calculations with the aim of examining the sensitivity of the theoretical LPV to the parameters of the new OPM. Fig. 15 illustrates the modifications of profile variations due to changes of the amplitude and phase of the linewidth oscillations and due to changes of the angle  $\alpha$  between the line of sight and pulsation axis. Gradual increase of the linewidth amplitude transforms symmetric, S-shaped LPV into asymmetric, blue-to-red pattern (see Fig. 15a). Thus, the diversity and height dependence of the LPV observed in roAp stars can be plausibly attributed to different  $V_p - \delta W$  combinations and to a growth of the linewidth amplitude with height. Qualitative comparison of the simulated profile time series and observations suggests that for most stars  $\delta W$  lies in the range from 0 to 1.5–2  $\text{km s}^{-1}$ . Fig. 15(a) also demonstrates that the shape of the standard deviation profile changes from a double peak to single peak when  $\delta W$  is increased. This agrees with our observations of the correlation between LPV pattern and the standard deviation shape. The fact that we never observe a dominant central peak in the standard deviation signatures also points to  $\delta W$  amplitudes below 1.5–2  $\text{km s}^{-1}$ .

Changing the  $\varphi_W$  parameter from 0 to  $\approx 0.15$  also strongly affects the LPV character. Fig. 15(b) clearly shows that it is a non-zero

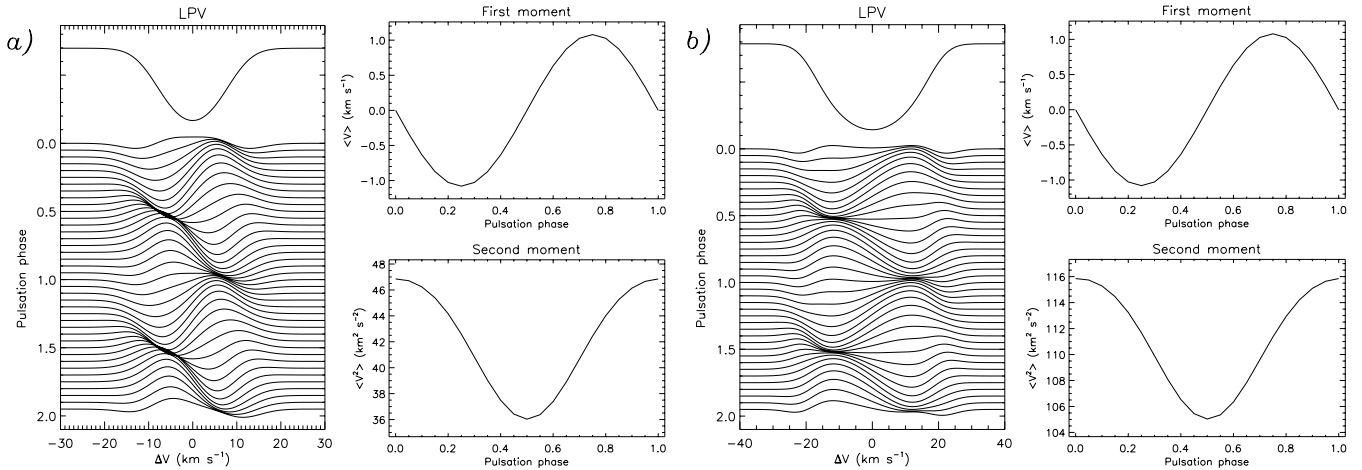


**Figure 14.** The same as in Fig. 6(b) for the oblique non-radial pulsator with (a)  $v_e \sin i = 10 \text{ km s}^{-1}$  and (b)  $v_e \sin i = 20 \text{ km s}^{-1}$ .

phase shift between the velocity and linewidth oscillation that introduces an asymmetry in LPV. The blue-to-red shifting features are obtained for positive  $\varphi_W$  exceeding  $\approx 0.1$ . On the other hand, negative  $\varphi_W$  results in the opposite, red-to-blue, pattern, possibly detected in Nd II lines of HD 9289. The morphology of the LPV is relatively unaffected by variation of the phase shifts between 0.15 and 0.35. Interestingly, a  $\varphi_W$  different from 0 and 0.25 produces an asymmetric standard deviation, which is sometimes shifted with respect to the line centre. This provides the first explanation of the origin of distorted and shifted standard deviation profiles frequently observed in slowly rotating roAp stars.

Rotational modulation of the LPV pattern presented in Fig. 15(c) shows a small change of profile variation as the line of sight shifts from the pulsation pole to the pulsation equator of the oblique dipolar mode. A dramatic change of the LPV is associated with a narrow range of rotation phases around  $\alpha = 90^\circ$ , when the mode is viewed equator-on. For this pulsation geometry, the RV variation is negligible and LPV is caused entirely by the linewidth oscillations.

The LPV calculations presented in this section convincingly demonstrate the success of our new OPM. Simultaneous pulsational variation of velocity and linewidth naturally explains a wide range of the LPV behaviour observed in roAp stars. We showed that, by adjusting a few parameters (amplitude and phase of the linewidth variation) of our model, it becomes possible to reproduce the diverse variations found for different groups of REE lines.

### 5.3 A shock wave signatures in the LPV of roAp stars?

Recently, another interpretation of pulsational profile variations in roAp stars was proposed by Shibahashi et al. (2004). These authors suggested that the smooth, blue-to-red shift observed by Kochukhov & Ryabchikova (2001a) in the LPV of the Nd III 6145 Å line in  $\gamma$  Equ represents the signature of shock waves propagating in the high atmospheric layers. Shibahashi et al. deduce the velocity of the pulsation wave, not from the amplitude of the RV oscillation ( $\approx 500 \text{ m s}^{-1}$  for this Nd III line), but from the full span of the residual profile variation (see Fig. 1). This gives a maximum speed of  $\sim 18 \text{ km s}^{-1}$ , which is substantially higher than the sound speed. Based on these arguments, Shibahashi et al. claim that LPV is affected by shocks and the harmonic time dependence in equation (3)

should be replaced by a saw-tooth law typical for large-amplitude non-linear stellar oscillations.

We believe that the basic assumption of Shibahashi et al. (2004) is incorrect because it is based on an erroneous interpretation of the pulsational profile distortions in terms of the physical velocity of the pulsation wave. The velocity span of the residual profile variation is determined by a convolution of the intrinsic stellar line profile with the pulsation velocity field. If the former is large compared to the pulsation velocity amplitude, as is the case for REE lines in roAp stars, the velocity span of LPV is not representative of the true pulsation wave speed. This situation is analogous to the behaviour of rapidly rotating non-radial pulsators, where profile variation with  $V_p \ll v_e \sin i$  is observed in the whole velocity range from  $-v_e \sin i$  to  $+v_e \sin i$  (Schrijvers et al. 1997). Thus, we assert that observations of  $\gamma$  Equ and other roAp stars give no evidence of supersonic pulsation velocity speeds and therefore the model of Shibahashi et al. (2004) cannot be correct.

However, it is still instructive to investigate the consequences of a non-sinusoidal velocity variation for oblique pulsators. In doing this, we have followed Shibahashi et al. (2004) and replaced the  $\exp(i\omega t)$  term of equation (3) by  $\sum_{n=1}^{10} n^{-1} \exp(in\omega t)$ . Additional moderate smoothing along the time axis is required to get rid of wiggles introduced by a finite number of terms in the latter expression. The line profile and moment variability resulting from a saw-tooth time dependence of the pulsation velocity is presented in Fig. 16. Evidently, the residual LPV shows a blue-to-red shift, which is superficially similar to the observed profile behaviour. However, the time series of residuals also shows a prominent gap due to the very fast evolution of the profile shape at phase 0. This is essentially the signature of the shock wave postulated by Shibahashi et al. (2004). No such rapid changes of line profiles have been reported for any roAp star. Also, in contradiction with observations, the variation of the line profile moments predicted by the shock wave model contains a large harmonic contribution. The observed phase relation of RV and linewidth is not reproduced either: the maximum linewidth coincides with the velocity extremum, whereas observations point to a 0.25 phase offset between the two curves.

In summary, our theoretical calculations suggest that, even putting aside the dubious foundation of the shock wave model, the line profile and moment variability predicted by this theory disagrees with observations. In our opinion, this proves that the model formulated

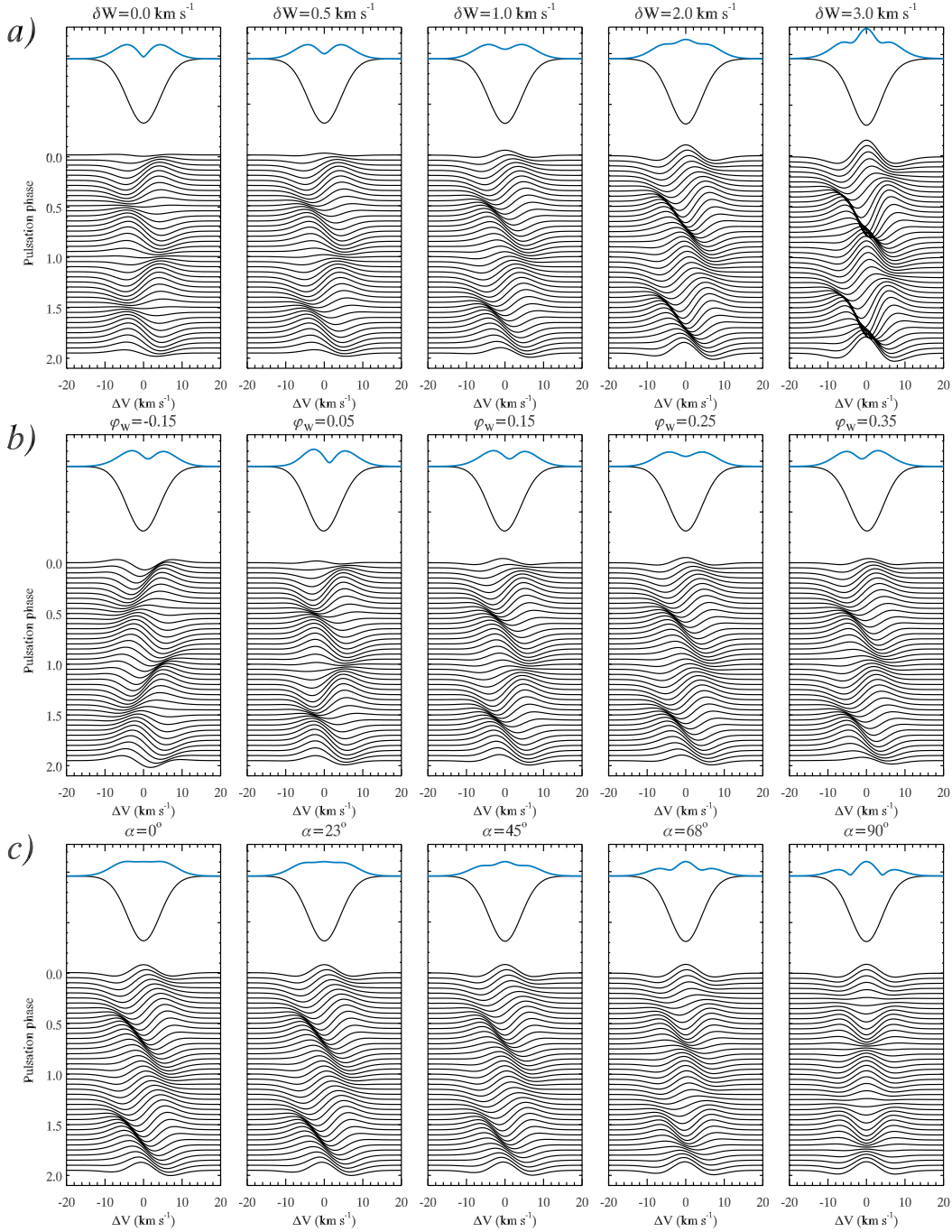


**Figure 15.** Dependence of the LPV pattern on (a) amplitude  $\delta W$  of the linewidth changes, (b) phase shift  $\varphi_w$  between the linewidth and pulsation velocity variability and (c) the angle  $\alpha$  between the pulsation axis and the line of sight. The standard set of the oblique pulsator parameters is  $\ell = 1, m = 0, V_p = 2.0 \text{ km s}^{-1}, K = 0, \delta W = 1.5 \text{ km s}^{-1}, \alpha = 0^\circ$ . In each subpanel, the average line profile and the standard deviation (arbitrary scale) are presented on top. The time-resolved difference spectra, covering two pulsation cycles, are plotted below.

by Shibahashi et al. (2004) does not provide a viable solution to the puzzle of LPV in roAp stars.

## 6 DISCUSSION

Our survey of pulsational line profile variability has, for the first time, characterized in detail the rapid fluctuations of REE lines in a representative sample of slowly rotating roAp stars. For a subset of lines in each star studied, we demonstrated the presence of asym-

metric LPV of the type first reported by Kochukhov & Ryabchikova (2001a) for  $\gamma$  Equ. We point out the close relation of this variability to the high-amplitude oscillation of the second moment. Both the asymmetric, blue-to-red shifting features in the residual profile time series, and the single-wave linewidth modulation with pulsation phase, increase rapidly with height and reach a maximum in the uppermost atmospheric layers, probed by strong doubly ionized REE lines. We show that this type of LPV is incompatible with the standard OPM, which attributes pulsational spectroscopic

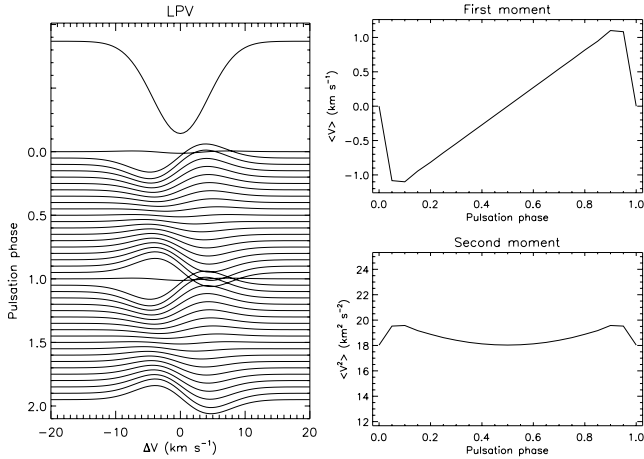


**Figure 16.** LPV expected for the oblique non-radial pulsator within the framework of the shock wave model proposed by Shibahashi et al. (2004). The velocity field geometry is that of the pole-on  $\ell = 1, m = 0, V_p = 1.6 \text{ km s}^{-1}$  pulsation mode. The temporal variation is given by the smoothed saw-tooth function  $\sum_{n=1}^{10} n^{-1} \exp(in\omega t)$ . Other parameters and the layout of the figure are the same as in Fig. 13(a).

variability to the velocity perturbations described by the  $\ell = 1, m = 0$  spherical harmonic. Extensive line profile calculations reveal that none of the recent modifications and extensions of the oblique pulsator framework (Bigot & Dziembowski 2002; Saio & Gautschy 2004; Cunha 2006), nor the exotic shock wave model of Shibahashi et al. (2004), are capable of explaining the LPV observed in sharp-lined roAp stars. Nevertheless, we show that theoretical LPV can be brought into remarkable agreement with experimental data if a pulsational modulation of the width of the local intrinsic spectral line profile is incorporated into the model. This new oblique pulsator framework is based on dipolar modes, and thus does not contradict observational evidence of the presence of this type of non-radial oscillations, accumulated by numerous previous spectroscopic and photometric studies of roAp stars. At the same time, a combination of the velocity and linewidth variability solves the puzzle of asymmetric LPV, explains why this line profile behaviour is clearly detected only in sharp-lined roAp stars, and provides a satisfactory interpretation of the line profile moments and the morphology of the standard deviation spectrum. The empirical success of our linewidth modulation hypothesis notwithstanding, the important question of the physical mechanism responsible for the pulsational alternation of the width of spectral lines has not yet been addressed. Here we attempt to shed light on this problem.

High-resolution, high-S/N observations of cool Ap stars reveal a number of line profile and line strengths anomalies, usually attributed to the combined effects of chemical stratification, a strong magnetic field, and non-solar chemical composition (Ryabchikova et al. 2002). However, the significant broadening of strong doubly ionized REE lines in slowly rotating cool Ap stars has received no satisfactory explanation so far. This problem is illustrated in Fig. 17 for the Nd III 6145 Å line in  $\gamma$  Equ. We compare the highest resolution observation of this star available in the ESO Archive (co-added  $\lambda/\Delta\lambda = 220\,000$  spectra obtained by Savanov et al. (2005)) with the magnetic spectrum synthesis calculations based on the stellar parameters, chemical abundances and magnetic field model of Ryabchikova et al. (2002). The additional broadening required to fit the Zeeman resolved components of the Fe II and Cr II lines is approximately  $2 \text{ km s}^{-1}$ . This is much smaller than  $V_{\text{macro}} \geq$

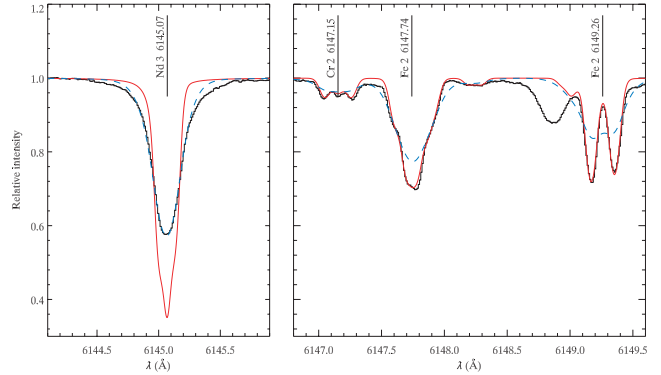


**Figure 17.** Comparison of very high resolution observation of  $\gamma$  Equ (thin curve) with magnetic spectrum synthesis calculations. Zeeman resolved profiles of the iron-peak lines (right-hand panel) are well reproduced with a macro-turbulent broadening of  $2 \text{ km s}^{-1}$  (thick solid curve). In contrast, a satisfactory fit to the broad wings of the Nd III 6145 Å line (left-hand panel) is only possible for  $V_{\text{macro}} \geq 10 \text{ km s}^{-1}$  (dashed curve).

$10 \text{ km s}^{-1}$  required to roughly reproduce the profile of the Nd III line. Such a high Gaussian smearing washes out the Zeeman structure in the Fe-peak lines and, therefore, contradicts observations of spectral lines formed in the lower atmosphere of  $\gamma$  Equ. The factor of 5 discrepancy in the best-fitting macro-turbulence derived for iron-peak elements and Nd III cannot be ascribed to isotope splitting or hyperfine structure effects (those are small for Nd III, see Dolk et al. (2002)) and seems to reflect a genuine increase of the isotropic velocity component towards the high-lying REE cloud.

Unusually strong broadening of pulsating REE lines was first discussed for  $\gamma$  Equ by Kochukhov & Ryabchikova (2001a). In that paper, we advocated a high- $\ell$ , non-axisymmetric mode in  $\gamma$  Equ and attributed the large broadening of Pr III and Nd III lines to the unresolved, large-amplitude pulsational velocity field. Our new investigation of this and other roAp stars suggests a different picture: pulsation modes are axisymmetric with  $\ell = 1$ , and linewidth modulation is invoked to explain the observed LPV. This model implies local pulsational perturbations with amplitudes not exceeding  $1\text{--}2 \text{ km s}^{-1}$  for the REE line-forming layer, which leaves no room for  $\sim 10 \text{ km s}^{-1}$  pulsational broadening in the time-averaged spectrum. Comparison of the pulsational amplitude and line broadening for different time-resolved spectroscopic data sets of  $\gamma$  Equ and for different roAp stars also argues against a direct relation between the average linewidth and non-radial pulsation. We also find no differences between the REE line broadening for time-averaged spectra obtained from time series of  $\gamma$  Equ characterized by an overall RV amplitude that is different by a factor of 5. Many roAp stars have relatively low ( $< 100 \text{ m s}^{-1}$ ) pulsation amplitudes (HD 137949, HD 166473, HD 176232) but, nevertheless, show very broad REE lines. Finally, apart from the small linewidth modulation discussed in this paper, no systematic reduction of the REE linewidths is observed in time-resolved spectra.

Thus, effects other than pulsational variability must be responsible for the inexplicable broadening of REE lines. Turbulence caused by convective instability is an obvious candidate for explanations of roAp-star observations. The location of cool Ap stars in the HR diagram coincides with Am stars, for which large broadening of strong lines is observed and interpreted as a signature of convective motions (Landstreet 1998). On the other hand, the intense magnetic fields of Ap stars are likely to modify and, possibly, suppress H and He convection zones. Ubiquitous signatures of chemical stratification also

indicate a lack of convective mixing in the lower atmosphere of cool Ap stars, though some mixing is required to reduce the discrepancy between theoretical diffusion models and observations (LeBlanc & Monin 2004). The message of these modern theoretical and observational results is that magnetic field–convection interaction in cool Ap stars is far more complex than previously thought and that a common assumption of the full suppression of convection is likely to be an oversimplification.

With this background, turbulence related to convective or pulsationally driven instability is the most plausible explanation of the anomalous broadening of REE lines. We speculate that some cool Ap stars, including the roAp pulsators studied in our paper, possess a turbulence zone in the upper atmospheric layers, roughly at the height of the REE-rich cloud. Large vertical gradients of chemical composition in the intermediate atmosphere ( $-3.5 \leq \log \tau_{5000} \leq -0.5$ ) exclude significant mixing. Therefore, turbulence should appear only in layers above  $\log \tau_{5000} \approx -3.5$  to  $-4.0$ . We find that strong REE lines often display excessive width of the outer wings, which is difficult to reproduce assuming a height-independent broadening parameter. Possibly, line cores sample layers with a weaker turbulence – a situation consistent with a decrease of convection efficiency with height.

At this stage we can offer no complete physical theory explaining the appearance of the turbulence zone in the upper atmospheres of cool Ap stars. One reason for the convective instability to develop may be a non-standard temperature structure of Ap-star atmospheres. Empirical evidence for this kind of anomaly was found by Kochukhov et al. (2002). By fitting the peculiar shape of the core-wing transition of the hydrogen Balmer lines, they derived semi-empirical models, characterized by a nearly flat temperature profile above  $\log \tau_{5000} \approx -1.0$  followed by a steep drop of temperature at  $\log \tau_{5000} \approx -4.0$ . This large temperature gradient may lead to convective instability<sup>2</sup> very close to the inferred location of the turbulence zone needed to explain broadening of REE lines.

What could be the response of the hypothetical turbulent layer to the non-radial p-mode oscillations? We know that the amplitude of convective motions grows as the mean atmospheric pressure increases (Heiter et al. 2002). Pulsational modulation of convection efficiency was invoked to explain observations for several classes of pulsating stars (Fokin, Gillet & Breitfellner 1996; Gillet et al. 1998). One usually infers that convective motions become stronger during the compression phase of the oscillation cycle. Conversely, convection is less intense during the expansion of the pulsating star. This is precisely the relationship between the linewidth and radius variation that we have deduced for roAp stars. Consequently, it is reasonable to suggest that pulsations modulate the efficiency of turbulence in the upper atmospheres of roAp stars, and this leads to the observed linewidth and LPV.

We hope that our interpretation of the pulsational LPV in roAp stars and the possible discovery of a new turbulence zone will stimulate new detailed magnetohydrodynamic modelling of the interaction between convection, pulsation and magnetic field in cool Ap stars. Three-dimensional radiative hydrodynamic simulations of A-star convection (e.g. Kochukhov et al. 2006) should be extended to include large-scale fossil magnetic fields. Variable lower boundary condition can be used to simulate the effects of high-overtone p modes. On the other hand, a NLTE semi-empirical analysis of hydrogen lines, coupled with model atmosphere calculations taking into account chemical stratification and the magnetic field (Shulyak

et al. 2004; Kochukhov, Khan & Shulyak 2005), is necessary to verify and extend the results of Kochukhov et al. (2002).

## ACKNOWLEDGMENTS

This paper is based on observations obtained at the European Southern Observatory (Paranal, Chile) and at the CFHT. Resources provided by the electronic data bases (VALD, SIMBAD, NASA's ADS) are acknowledged. Our research is supported by the grants from the Swedish Kungliga Fysiografiska Sällskapet, Swedish Royal Academy of Sciences (project 11630102), Russian Foundation for Basic Research (project 04-02-16788a), the Austrian Science Fund (project P17580) and the Natural Sciences and Engineering Research Council of Canada.

## REFERENCES

- Aerts C., Waelkens C., 1993, *A&A*, 273, 135  
 Aerts C., De Pauw M., Waelkens C., 1992, *A&A*, 266, 294  
 Babel J., 1992, *A&A*, 258, 449  
 Balona L. A., 1986, *MNRAS*, 219, 111  
 Balona L. A., 2002, *MNRAS*, 337, 1059  
 Biémont E., Palmeri P., Quinet P., 1999, *Ap&SS*, 269–270, 635  
 Bigot L., Dziembowski W. A., 2002, *A&A*, 391, 235  
 Briquet M., Aerts C., 2003, *A&A*, 398, 687  
 Cowley C. R., Ryabchikova T., Kupka F., Bord D. J., Mathys G., Bidelman W. P., 2000, *MNRAS*, 317, 299  
 Cunha M. S., 2006, *MNRAS*, 365, 153  
 Dolk L., Wahlgren G. M., Lundberg H., Li Z. S., Litzén U., Ivarsson S., Ilyin I., Hubrig S., 2002, *A&A*, 385, 111  
 Fokin A. B., Gillet D., Breitfellner M. G., 1996, *A&A*, 307, 503  
 Gillet D., Debieve J. F., Fokin A. B., Mazauric S., 1998, *A&A*, 332, 235  
 Heiter U. et al., 2002, *A&A*, 392, 619  
 Kanaan A., Hatzes A. P., 1998, *ApJ*, 503, 848  
 Kochukhov O., 2004a, *A&A*, 423, 613  
 Kochukhov O., 2004b, *ApJ*, 615, L149  
 Kochukhov O., 2005, *A&A*, 438, 219  
 Kochukhov O., 2006, *A&A*, 446, 1051  
 Kochukhov O., Ryabchikova T., 2001a, *A&A*, 374, 615  
 Kochukhov O., Ryabchikova T., 2001b, *A&A*, 377, L22  
 Kochukhov O., Bagnulo S., Barklem P. S., 2002, *ApJ*, 578, L75  
 Kochukhov O., Ryabchikova T., Piskunov N., 2004, *A&A*, 415, L13  
 Kochukhov O., Khan S., Shulyak D., 2005, *A&A*, 433, 671  
 Kochukhov O., Freytag B., Piskunov N., Steffen M., 2006, in Kupka F., Roxburgh I. W., Chan K. L., eds, *IAU Symp. 239, Convection in Astrophysics*, in press  
 Kupka F., Ryabchikova T. A., Weiss W. W., Kuschnig R., Rogl J., Mathys G., 1996, *A&A*, 308, 886  
 Kupka F., Piskunov N., Ryabchikova T. A., Stempels H. C., Weiss W. W., 1999, *Ap&SS*, 138, 119  
 Kurtz D. W., 1982, *MNRAS*, 200, 807  
 Kurtz D. W., Martinez P., 2000, *Balt. Astron.*, 9, 253  
 Kurtz D. W., Sullivan D. J., Martinez P., Tripe P., 1994, *MNRAS*, 270, 674  
 Kurtz D. W., Elkin V. G., Mathys G., Riley J., Cunha M. S., Shibahashi H., Kambe E., 2004, in Zverko J., Žižňovský J., Adelman S. J., Weiss W. W., eds, *IAU Symp. 224, The A-star Puzzle* Cambridge Univ. Press, Cambridge, p. 343  
 Kurtz D. W., Elkin V. G., Mathys G., 2006, *MNRAS*, 370, 1274  
 Landstreet J. D., 1998, *A&A*, 338, 1041  
 LeBlanc F., Monin D., 2004, in Zverko J., Žižňovský J., Adelman S. J., Weiss W. W., eds, *IAU Symp. 224, The A-star Puzzle*. Cambridge Univ. Press, Cambridge, p. 193  
 Mashonkina L., Ryabchikova T., Ryabtsev A., 2005, *A&A*, 441, 309  
 Mathias P., Aerts C., de Pauw M., Gillet D., Waelkens C., 1994, *A&A*, 283, 813  
 Mkrtychian D. E., Hatzes A. P., Kanaan A., 2003, *MNRAS*, 345, 781

<sup>2</sup> We thank Dr. H. Saio for drawing our attention to this fact.

- Moon T. T., Dworetzky M. M., 1985, *MNRAS*, 217, 305  
Napiwotzki R., Schoenberner D., Wenske V., 1993, *A&A*, 268, 653  
Piskunov N., Kochukhov O., 2002, *A&A*, 381, 736  
Ryabchikova T. A., Landstreet J. D., Gelbmann M. J., Bolgova G. T.,  
Tsybal V. V., Weiss W. W., 1997, *A&A*, 327, 1137  
Ryabchikova T. A., Savanov I. S., Hatzes A. P., Weiss W. W., Handler G.,  
2000, *A&A*, 357, 981  
Ryabchikova T., Piskunov N., Kochukhov O., Tsybal V., Mittermayer P.,  
Weiss W. W., 2002, *A&A*, 384, 545  
Ryabchikova T., Nesvacil N., Weiss W. W., Kochukhov O., Stütz Ch., 2004,  
*A&A*, 423, 705  
Ryabchikova T. et al., 2005, *A&A*, 429, L55  
Ryabchikova T., Ryabtsev A., Kochukhov O., Bagnulo S., 2006, *A&A*, 456,  
329  
Ryabchikova T. et al., 2007, *A&A*, 462, 1103  
Saio H., 2005, *MNRAS*, 360, 1022  
Saio H., Gautschy A., 2004, *MNRAS*, 350, 485  
Savanov I. S., Malanushenko V. P., Ryabchikova T. A., 1999, *Astron. Lett.*,  
25, 802  
Savanov I. S., Hubrig S., Mathys G., Ritter A., Kurtz D. W., 2005, *A&A*,  
448, 1165  
Schrijvers C., Telting J. H., Aerts C., Ruymaekers E., Henrichs H. F., 1997,  
*A&AS*, 121, 343  
Shibahashi H., Kurtz D. W., Kambe E., Gough D. O., 2004, in Zverko J.,  
Žižňovský J., Adelman S. J., Weiss W. W., eds, *IAU Symp. 224, The  
A-star Puzzle*. Cambridge Univ. Press, Cambridge, p. 829  
Shulyak D., Tsybal V., Ryabchikova T., Stütz Ch., Weiss W. W., 2004,  
*A&A*, 428, 993  
Smeyers P., Tassoul M., 1987, *ApJS*, 65, 429  
Tsybal V., Lyashko D., Weiss W. W., 2003, in Piskunov N., Weiss W. W.,  
Gray D. F., eds, *IAU Symp. 210, Modelling of Stellar Atmospheres*.  
*Astron. Soc. Pac.*, San Francisco, p. E49

This paper has been typeset from a  $\text{\TeX}/\text{\LaTeX}$  file prepared by the author.